Sensitivity of polar stratospheric cloud formation to changes in water vapour and temperature

(article starts on next page)

Atmospheric
Chemistry
and Physics

Sensitivity of polar stratospheric cloud formation to changes in water vapour and temperature

F. Khosrawi[1,a], **J. Urban**[2,†], **S. Lossow**[3], **G. Stiller**[3], **K. Weigel**[4], **P. Braesicke**[3], **M. C. Pitts**[5], **A. Rozanov**[4], **J. P. Burrows**[4], **and D. Murtagh**[2]

[1]Department of Meteorology, Stockholm University, Stockholm, Sweden
[2]Department of Earth and Space Science, Chalmers University of Technology, Gothenburg, Sweden
[3]Institute of Meteorology and Climate Research, Karlsruhe Institute of Technology, Karlsruhe, Germany
[4]Institute of Environmental Physics, University of Bremen, Bremen, Germany
[5]NASA Langley Research Center, Hampton, USA
[a]now at: Institute of Meteorology and Climate Research, Karlsruhe Institute of Technology, Karlsruhe, Germany
[†]deceased, 14 August 2014

Correspondence to: F. Khosrawi (farahnaz.khosrawi@kit.edu)

Abstract. More than a decade ago it was suggested that a cooling of stratospheric temperatures by 1 K or an increase of 1 ppmv of stratospheric water vapour could promote denitrification, the permanent removal of nitrogen species from the stratosphere by solid polar stratospheric cloud (PSC) particles. In fact, during the two Arctic winters 2009/10 and 2010/11 the strongest denitrification in the recent decade was observed. Sensitivity studies along air parcel trajectories are performed to test how a future stratospheric water vapour (H_2O) increase of 1 ppmv or a temperature decrease of 1 K would affect PSC formation. We perform our study based on measurements made during the Arctic winter 2010/11. Air parcel trajectories were calculated 6 days backward in time based on PSCs detected by CALIPSO (Cloud Aerosol Lidar and Infrared Pathfinder satellite observations). The sensitivity study was performed on single trajectories as well as on a trajectory ensemble. The sensitivity study shows a clear prolongation of the potential for PSC formation and PSC existence when the temperature in the stratosphere is decreased by 1 K and water vapour is increased by 1 ppmv. Based on 15 years of satellite measurements (2000–2014) from UARS/HALOE, Envisat/MIPAS, Odin/SMR, Aura/MLS, Envisat/SCIAMACHY and SCISAT/ACE-FTS it is further investigated if there is a decrease in temperature and/or increase of water vapour (H_2O) observed in the polar regions similar to that observed at midlatitudes and in the tropics. Performing linear regression analyses we derive from the Envisat/MIPAS (2002–2012) and Aura/MLS (2004–2014) observations predominantly positive changes in the potential temperature range 350 to 1000 K. The linear changes in water vapour derived from Envisat/MIPAS observations are largely insignificant, while those from Aura/MLS are mostly significant. For the temperature neither of the two instruments indicate any significant changes. Given the strong inter-annual variation observed in water vapour and particular temperature the severe denitrification observed in 2010/11 cannot be directly related to any changes in water vapour and temperature since the millennium. However, the observations indicate a clear correlation between cold winters and enhanced water vapour mixing ratios. This indicates a connection between dynamical and radiative processes that govern water vapour and temperature in the Arctic lower stratosphere.

1 Introduction

Polar stratospheric clouds (PSCs) form in the polar winter stratosphere at altitudes between 15 to 30 km. PSCs consist of liquid and solid particles and have been classified into three different types based on their composition and physical state: (1) supercooled ternary solutions (STS), (2) Nitric

Acid Trihydrate (NAT) and (3) ice. The formation of PSCs is strongly temperature dependent. Liquid PSC cloud particles (STS) form by the condensation of water vapour (H$_2$O) and nitric acid (HNO$_3$) on the liquid stratospheric background sulfate aerosol particles at temperatures 2–3 K below the NAT existence temperature T_{NAT} ($\sim$ 195 K at 20 km) while for the formation of solid cloud particles (ice) much lower temperatures are required, usually 3–4 K below the ice frost point T_{ice} ($\sim$ 185 K at 20 km) (e.g. Carslaw et al., 1994; Koop et al., 1995). The formation of the liquid STS particles is quite well understood, however, the exact formation mechanism of NAT and ice PSC particles still leaves some unresolved questions and is still an active area of research.

Progress in understanding PSC particle formation processes has been made recently in the frame of the European project RECONCILE (Reconciliation of essential process parameters for an enhanced predictability of Arctic stratospheric ozone loss and its climate interactions) (von Hobe et al., 2013). For example, CALIPSO measurements for the Arctic winter 2009/10 presented by Pitts et al. (2011) showed that widespread NAT formation occurred, albeit in low number densities, before ice clouds had been formed at temperatures well above T_{ice}. Further, lidar measurements performed during recent years have also indicated that there must be a formation mechanism for NAT PSCs above the ice frost point T_{ice} without ice particles necessarily serving as a nucleation kernel for NAT particles. Until the RECONCILE project, the only known pathway to form NAT was through heterogeneous nucleation on ice particles, forming NAT clouds downstream of mountain wave ice clouds (Luo et al., 2003; Fueglistaler et al., 2003; Höpfner et al., 2006).

Heterogeneous nucleation on particles such as meteoric smoke has been suggested to be a potential pathway for NAT formation (Bogdan et al., 2003; Voigt et al., 2005). Hoyle et al. (2013) performed box model simulations along air parcel trajectories based on the observations by CALIPSO made during the Arctic winter 2009/10 applying a new parameterisation for heterogeneous NAT nucleation, assuming NAT formation on particles as e.g. meteoric smoke. The CALIPSO observations were well reproduced by the model simulations applying this new parameterisation thus indicating that NAT nucleation on other particles than ice is possible. Further, both the modelling study by Hoyle et al. (2013) and the one by Engel et al. (2013) using the Zurich Optical and Microphysical box Model (ZOMM) showed that small-scale temperature fluctuations usually not represented in meteorological data needed to be considered to reproduce the CALIPSO observations.

Denitrification, the permanent removal of HNO$_3$ by sedimenting polar stratospheric cloud particles, limits the deactivation process of the ozone destroying substances in springtime and thus leads to a prolongation of the ozone destroying cycles. Stratospheric cooling caused by increasing greenhouse gas concentrations will have significant implications on denitrification and ozone loss. Model simulations predict

that very large ozone losses will occur more frequently in the future in the Arctic and that the recovery of the ozone layer will be delayed by more than a decade due to increased greenhouse gas concentrations (e.g. Austin et al., 1992; Shindell et al., 1998; Eyring et al., 2010; SPARC CCMVal, 2010).

Water vapour is one of the most important greenhouse gases and plays a key role in the chemistry and radiative balance of the upper troposphere and lower stratosphere (UT/LS). Several studies have been performed in the past investigating stratospheric water vapour trends using in situ and remote-sensing measurements (e.g. Oltmans et al., 2000; Rosenlof et al., 2001; Hurst et al., 2011; Hegglin et al., 2014). Rosenlof et al. (2001) combined 10 data sets covering the time period 1954–2000 and found a 1 % yr^{-1} (0.054 ppmv yr^{-1}) increase in lower stratospheric water vapour in the mid-latitudes. Long-term balloon-borne measurements at Boulder, Colorado (40° N/105° W) indicate an increase of lower stratospheric water vapour abundances, on average by 1 ppmv, during the last 30 years (1980–2010) (Scherer et al., 2008; Hurst et al., 2011). Recently, Hegglin et al. (2014) analysed a merged satellite time series spanning from the late 1980s to 2010, which did not confirm the findings from the Boulder data set, arguing the representativeness of these data on a larger spatial scale. In the lower stratosphere negative changes were dominating, while positive changes were found only in the upper part of the stratosphere. The decrease in the lower stratosphere was attributed to a strengthened lower stratospheric circulation. A decisive role here played a pronounced drop in water vapour in 2000 (also known as the millennium drop) (Randel et al., 2006; Scherer et al., 2008; Solomon et al., 2010; Urban et al., 2012), that first started to recover in 2004 to 2005. This drop was caused by a reduced transport of water vapour from the troposphere into the stratosphere in response to a colder tropical tropopause. The temperature decrease has been due to variations of the QBO (quasi-biennial oscillation), ENSO (El Niño Southern Oscillation) and the Brewer-Dobson circulation that collectively acted in the same direction lowering the tropopause temperatures. In 2011 such a drop happened again, however more short-lived (Urban et al., 2014).

Dessler et al. (2014) analysed satellite data together with a trajectory model. They did not see any firm evidence of trends (neither positive nor negative) in the data since the mid 1980s. However, they cannot rule out that a trend exists that is just too small to be identified given the large interannual and inter-decadal variability. Gettelman et al. (2010) presented model simulations of 18 coupled Chemistry Climate Models (CCMs) in the tropical tropopause layer (TTL). The models simulate decreases in the tropopause pressure in the 21st century, along with $\sim$ 1 K increases per century in cold point temperature and 0.5–1 ppmv per century increases in water vapour above the tropical tropopause.

Any changes in atmospheric water vapour bring important implications for the global climate. Increases in stratospheric water vapour cool the stratosphere but warm the troposphere.

Both the cooling of the stratosphere and the increase in water vapour enhance the potential for the formation of polar stratospheric clouds. More than a decade ago it was already suggested that a cooling of stratospheric temperatures by 1 K or an increase of 1 ppmv of stratospheric water vapour could promote denitrification (Santee et al., 1995; Tabazadeh et al., 2000). During the two Arctic winters 2009/10 and 2010/11, the strongest denitrification in the recent decade was observed (Khosrawi et al., 2011, 2012). In the latter winter, denitrification led also to severe ozone depletion with a magnitude comparable to the Antarctic "ozone hole" (Manney et al., 2011; Sinnhuber et al., 2011; Arnone et al., 2012; Kuttipurath et al., 2012; Hommel et al., 2014).

In this study, the correlation between observed water vapour variability and the recent temperature evolution in the Arctic together with PSC observations are considered to investigate a possible connection between the increase in stratospheric water vapour and polar stratospheric cloud formation/denitrification. This study aims at (1) performing a sensitivity study on how an increase in water vapour and decrease in temperature will affect PSC formation and existence and (2) on assessing the H$_2$O variability during the 15-year period 2000–2014.

1. A sensitivity study is performed to investigate what effect changes in water vapour and temperature (due to a trend or variability) would have on PSC formation and occurrence. Therefore, air parcel back trajectories are calculated according to PSC observations by CALIPSO during the Arctic winter 2010/11. On the basis of this trajectory ensemble the increase in time the air parcels would be exposed to temperatures below T_{NAT} or T_{ice} along the trajectories are considered for a water vapour increase of up to 1 ppmv and a temperature decrease of up to 1 K in the stratosphere.

2. Measurements from several different satellites together with temperatures from ECMWF are used to investigate water vapour trends and variability in the polar stratosphere. So far trend studies in stratospheric water vapour have focused on the tropics and mid-latitudes. Here, for the first time such an analysis has been performed for the polar stratosphere. We use satellite measurements that were derived for the 15-year period 2000–2014.

2 Satellite data

To investigate a possible water vapour trend as well as water vapour variability in the polar lower stratosphere, satellite observations of water vapour from the Odin Sub-Millimetre Radiometer (Odin/SMR), the Aura Microwave Limb Sounder (Aura/MLS), the Envisat Michelson Interferometer for Passive Soundings (Envisat/MIPAS), the Scanning Imaging Absorption spectrometer for Atmospheric

Chartography (Envisat/SCIAMACHY), the SCISAT Atmospheric Chemistry Experiment Fourier Transform Spectrometer (SCISAT/ACE-FTS) and the UARS Halogen Occultation Experiment (UARS/HALOE) are used. A short description of these satellite instruments will follow below. A detailed intercomparison of water vapour derived from these instruments can be found in Hegglin et al. (2013). For performing case studies along air parcel trajectories that are based on PSC measurements we apply measurements from the Cloud-Aerosol Lidar with Orthogonal Polarization (CALIOP) on board of CALIPSO (Cloud-Aerosol Lidar and Infrared Pathfinder Satellite Observations).

2.1 Odin/SMR

Odin/SMR was launched on 20 February 2001 and it observes the thermal emission of trace gases from the Earth's limb. Odin carries two instruments, the Optical Spectrograph and Infrared Imaging System (OSIRIS) (Llewellyn et al., 2004) and the Sub-Millimetre Radiometer (SMR) (Frisk et al., 2003). Observations by Odin/SMR were performed in a time-sharing mode with astronomical observations until 2007 and solely in aeronomy mode thereafter. In aeronomy mode, various target bands are dedicated to profile measurements of trace constituents relevant to stratospheric and mesospheric chemistry and dynamics such as O$_3$, ClO, N$_2$O, HNO$_3$, H$_2$O, CO, HO$_2$ and NO, as well as minor isotopologues of H$_2$O and O$_3$ (e.g. Murtagh et al., 2002). Stratospheric mode measurements were performed every third day until April 2007 and every other day thereafter. A typical stratospheric mode scan covers the altitude range from 7 to 70 km with a resolution of $\sim$ 1.5 km in terms of tangent altitude below 50 km and of $\sim$ 5.5 km above. Usually, the latitude range between 82.5° S and 82.5° N is observed (Urban et al., 2005b, a). Water vapour measurements are derived by Odin/SMR in several different bands in the sub-millimetre range. Here, level-2 data from the 544.6 GHz band of version 2.0 for the lower stratosphere are used (Urban et al., 2007, 2012; Urban, 2008).

2.2 Aura/MLS

MLS on board Aura is part of the NASA/ESA "A-train" satellite constellation. MLS was launched in July 2004 and is an advanced successor of the MLS instrument on the Upper Atmosphere Research Satellite (UARS) that was launched in 1991 and provided measurements until 1999. MLS is a limb sounding instrument that measures the thermal emission at millimetre and sub-millimetre wavelengths using seven radiometers to cover five broad spectral regions (Waters et al., 2006). Measurements are performed from the surface to 90 km with a global latitude coverage from 82° S to 82° N. Global water vapour measurements are derived from a line close to the 183 GHz band (Lambert et al., 2007). Version 3.3 data is used in this study (Hurst et al., 2014).

2.3 Envisat/MIPAS

MIPAS is a middle infrared Fourier transform spectrometer and was launched in March 2002 on board Envisat. MIPAS was operational until the sudden loss of contact with Envisat on 8 April 2012. MIPAS measured the atmospheric emission spectrum in the limb sounding geometry. MIPAS operated in its nominal observation mode from June 2002 to March 2004, thus approximately 2 years. Measurements during this time period were performed in its full spectral resolution measurement mode with a designated spectral resolution of 0.035 cm^{-1}. Measurements were performed covering the altitude range from the mesosphere to the troposphere with a high vertical resolution (about 3 km in the stratosphere). After a failure of the interferometer slide at the end of March 2004, MIPAS resumed measurements in January 2005 with a reduced spectral resolution of 0.0625 cm^{-1}, but with improved spatial resolution. Data products of MIPAS are up to 30 trace species, e.g. H$_2$O, O$_3$, HNO$_3$, CH$_4$, N$_2$O, NO$_2$ as well as temperature (Fischer and Oelhaf, 1996; Fischer et al., 2008). Here, the MIPAS data version V5H_H2O_20 and V5R_H2O_220/221 derived with the IMK/IAA retrieval processor covering the periods 2002–2003 and 2005–April 2011/May 2011–2012, respectively, have been used (updated version of the retrieval as described in Milz et al., 2009; von Clarmann et al., 2009).

2.4 Envisat/SCIAMACHY

SCIAMACHY was launched on board Envisat in March 2002 and was in operation from August 2002 until the sudden loss of contact with Envisat on 8 April 2012. SCIAMACHY observed electromagnetic radiation upwelling from the Earth's atmosphere in three measurement modes: occultation, nadir, and limb geometry. The instrument and mission objectives are provided by Burrows et al. (1995) and Bovensmann et al. (1999). In this study, measurements of the scattered solar light in limb viewing geometry are used. In this geometry, the instrument scanned the horizon in 3.3 km steps from −3 to 92 km (0 to 92 km since October 2010). This vertical sampling and the instantaneous field of view ($\sim$ 2.6 km in vertical direction at the tangent point) resulted in a vertical resolution of typically 3–4 km. Envisat was in a Sunsynchronous orbit with an inclination of 98°. This resulted in global coverage for SCIAMACHY limb measurements being achieved within 6 days at the Equator and less elsewhere (Gottwald et al., 2006). SCIAMACHY target species are O$_3$, BrO, OClO, ClO, SO$_2$, H$_2$CO, NO$_2$, CO, CO$_2$, CH$_4$, H$_2$O, N$_2$O, aerosol and clouds. In the limb viewing geometry water vapour is retrieved at about 10 to 25 km altitude from the near-infrared spectral range (1353–1410 nm). Here, we use SCIAMACHY water vapour from data version 3.01. The IUP Bremen water vapour retrieval algorithm V3.01 follows the retrieval concept presented in Rozanov et al. (2011) for V3 and the new data set is described in Weigel et al. (2015).

2.5 SCISAT/ACE-FTS

The ACE mission was launched on 12 August 2003 on-board the SCISAT satellite. SCISAT is a Canadian-led satellite mission and carries two instruments, the ACE Fourier Transform Spectrometer (ACE-FTS) and the Measurement of Aerosol Extinction in the Stratosphere and Troposphere Retrieved by Occultation (ACE-MAESTRO). ACE-FTS is a solar occultation instrument and has been providing measurements since 2004 (Bernath et al., 2005). Measurements are performed during sunrise and sunset (resulting in 15 sunrise and 15 sunset measurements per day). A seasonally varying coverage of the globe is provided, with an emphasis on mid-latitudes and the polar regions. The ACE-FTS measurements provide vertical profiles of more than 30 atmospheric species as well as temperature and pressure. The 14 baseline atmospheric species measured by ACE-FTS are O$_3$, H$_2$O, HCl, CCl$_3$F, CCl$_2$F$_2$, CH$_4$, HF, N$_2$O, CO, NO, NO$_2$, HNO$_3$, ClONO$_2$, and N$_2$O$_5$ (Boone et al., 2005). ACE-FTS version 3.5 data have been used in this study.

2.6 UARS/HALOE

The Halogen Occultation Experiment (HALOE) was launched aboard the Upper Atmosphere Research Satellite (UARS). HALOE is as ACE-FTS a solar occultation instrument (Russell et al., 1993). The geometry of the UARS orbit (57° inclination, circular at 585 km with orbit period of 96 min) results in 15 sunrise and 15 sunset measurements daily. Measurements between 80° N and 80° S in about 45 days are performed. HALOE was launched in September 1991 and provided measurements until 2005, thus over a time period of 14 years (Harris et al., 1996). Therefore, HALOE provides the longest satellite data set though it is not used to its full extent in this study since we focus on measurements obtained since the millennium. HALOE Version 19 data are used in this study.

2.7 CALIPSO/CALIOP

CALIPSO is part of the NASA/ESA "A-train" satellite constellation and has been in operation since June 2006. Measurements of PSCs are provided by CALIOP (Pitts et al., 2009). CALIOP is a two-wavelength, polarisation sensitive lidar. High vertical resolution profiles of the backscatter coefficient at 532 and 1064 nm as well as two orthogonal (parallel and perpendicular) polarisation components at 532 nm are provided (Winker et al., 2007; Pitts et al., 2007). The lidar pulse rate is 20.25 Hz, corresponding to one profile every 333 m horizontally. The vertical resolution of CALIOP varies with altitude from 30 m in the lower troposphere to 180 m in the stratosphere. For the PSC analyses, the CALIPSO profile data are averaged to a resolution of 180 m vertically and 5 km horizontally. The determination of the composition of PSCs is based on the measured aerosol depolarisa-

tion ratio (ratio of parallel and perpendicular components of 532 nm backscatter) and the inverse scattering ratio ($1/R_{532}$), where R_{532} is the ratio of the total to molecular backscatter at 532 nm (Pitts et al., 2007, 2009). Using these two quantities, PSCs are classified into STS, water ice, and three classes of liquid/NAT mixtures (Mix-1, Mix-2 and Mix-2 enhanced). Mix-1 denotes mixtures with very low NAT number densities (from about 3×10^{-4} to 10^{-3} cm^{-3}), Mix-2 denotes mixtures with intermediate NAT number densities of (10^{-3} cm^{-3}), and Mix-2 enhanced denotes mixtures with sufficiently high NAT number densities (> 0.1 cm^{-3}) and volumes (> 0.5 µm^3 cm^{-3}) that their presence is not masked by the more numerous STS droplets at temperatures well below T_{NAT}. In addition, intense mountain-wave induced ice PSCs are identified as a subset of CALIPSO ice PSCs through their distinct optical signature in R_{532} (Pitts et al., 2011).

3   Arctic winter 2010/11

The Arctic winter 2010/11 was one of the coldest in the last 2 decades (Manney et al., 2011; Sinnhuber et al., 2011). The 2010/11 winter was characterised by an anomalously strong vortex with an atypically long cold period that was persistent from mid-December to mid-March (Manney et al., 2011). The polar vortex formed at the end of November 2010 and remained stable until the end of April. The long cold period, lasting over 4 months, was interrupted by short warmer periods in the beginning of January, February and March due to minor warmings. In February and March, temperatures were colder than in previous years of the last decade. The final warming during the 2010/11 Arctic winter occurred in mid-April, thus later than usual (Arnone et al., 2012; Kuttipurath et al., 2012).

The PSC season during the 2010/11 winter can be divided into four PSC phases according to the four cold phases that occurred over the 4-month period from December 2010 to March 2011. The time periods of these four phases and the PSC types that occurred during each phase were derived from CALIPSO observations and are as follows (Khosrawi et al., 2012): (1) 23 December 2010 to 8 January 2011: STS, Mix 1/2 and ice clouds. (2) 20–28 January 2011: mainly Mix-1 and Mix-2 with some STS and ice. (3) 5–27 February: STS, Mix-1 and Mix-2 as well as ice clouds. (4) 5–19 March: STS clouds (Note: no CALIPSO data are available from 8 to 13 March).

A graphic presentation of the temporal evolution of time, V_{PSC}, $T - T_{NAT}$ and several trace gases during this winter can be found in Arnone et al. (2012) and Kuttipurath et al. (2012). Arnone et al. (2012) performed a similar analysis on PSC occurrence as we did, but used MIPAS observations for PSC detection. They also derive four PSC phases from MIPAS, however with somewhat different time periods for each phase as the ones we derive from CALIPSO. Differences

in PSC detection between both instruments are caused by the different measurement principle (active lidar in the visible vs. passive spectroscopy in the infrared spectral region). CALIPSO generally detects PSCs in a greater fraction than MIPAS. This can be explained by the patchier nature of PSCs in the Arctic and the different spatial resolutions of the two instruments, which makes the clouds more likely to be detected by the CALIPSO lidar (Höpfner et al., 2009). The Arctic winter 2010/11 has been well analysed, especially with respect to ozone loss (Manney et al., 2011; Sinnhuber et al., 2011; Arnone et al., 2012; Kuttipurath et al., 2012; Hommel et al., 2014) while the dynamical perspective, thus the exceptional dynamical conditions of this winter so far were only discussed in detail by Hurwitz et al. (2011).

4   Sensitivity studies

The sensitivity study is performed based on measurements of PSCs by CALIPSO during the Arctic winter 2010/11. The basic approach is demonstrated on single trajectories, but the final results rely on a statistical assessment of a trajectory ensemble. Based on the PSCs observed by CALIPSO during the Arctic winter 2010/11 air parcel trajectories were calculated 6 days backwards with the NOAA HYSPLIT (Hybrid Single Particle Lagrangian Integrated Trajectory Model) model based on GDAS (Global Data Assimilation System) analyses[1]. GDAS analyses are provided by the National Center for Environmental Predictions (NCEP) four times a day (00:00, 06:00, 12:00 and 18:00 UTC) with a horizontal resolution of $1° \times 1°$ on 23 pressure levels (1000 to 20 hPa). An isentropic method was used for the calculation of vertical motion. The trajectories were started for each PSC detection at three different altitudes, corresponding to the bottom, middle and top of the cloud.

The Arctic winter 2010/11 has been chosen for the sensitivity study because it was one of the coldest Arctic winters leading to a high number of PSC occurrences. This makes the statistics more reliable than if we would have chosen a warmer winter with less PSC occurrences. During the Arctic winter 2010/11 PSCs were detected by CALIPSO on 47 days on 259 orbit tracks. In total, 738 trajectories were calculated based on the CALIPSO observations and considered for the sensitivity study on the trajectory ensemble. For the sensitivity study on single trajectories we selected two trajectories, one trajectory where temperatures below T_{NAT} were reached, but not below T_{ice} and one where temperatures below both, T_{NAT} and T_{ice}, were reached along the trajectory. Figure 1 shows a map with locations where the trajectories were started according to the PSCs detected by CALIPSO, colour coded by the four cold phases during the Arctic winter 2010/11. PSCs were observed around Greenland during Phase 1, during Phase 2 PSCs were observed over Russia and during Phase 3 over the entire Arctic. During Phase 4
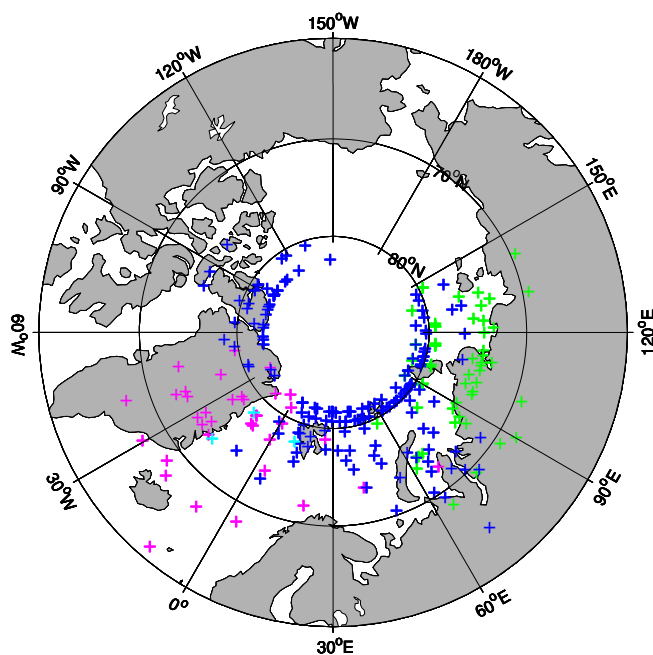
---

[1]http://ready.arl.noaa.gov/HYSPLIT.php

Figure 1. Start points where the back trajectories were started according to the PSCs observed by CALIPSO during the four cold phases during the Arctic winter 2010/11 (Phase 1: 23 December–8 January (magenta), Phase 2: 20–28 January (green), Phase 3: 5–27 February (blue) and Phase 4: 5–18 March (cyan)).

Table 1. Time periods when T_1 and T_2 were below the NAT and ice threshold temperature along the back trajectory. T_{NAT} and T_{ice} were derived for H$_2$O mixing ratios of 5, 5.5. and 6 ppmv for the trajectory started on 26 February 2011 at 00:00 UTC (Case 1). Only increases in water vapour were considered.

H$_2$O (ppmv)	$T_1 < T_{NAT}$ (h)	$T_2 < T_{NAT}$ (h)	$T_2 < T_{ice}$ (h)
5	40	20	–
5.5	41	20	–
6	42	20	–

cording to the parameterisations of Marti and Mauersberger (1993) and Hanson and Mauersberger (1988), respectively. T_{NAT} and T_{ice} were calculated for 5 ppmv (typical water mixing ratio during polar winter) and for increased water vapour mixing ratios of 5.5 and 6 ppmv, respectively. Along the trajectory temperatures drop twice below T_{NAT} (at $t = -140$ to -100 h, temperature range T_1, and at $t = -20$ to 0 h, temperature range T_2) but temperatures did not reach T_{ice}. The temperature range T_2 corresponds to the time period when a PSC was measured by CALIPSO on that day. The temperature drops sufficiently low below T_{NAT} to allow STS formation, which is in agreement with the CALIPSO observation at 20 km (Fig. 2). Although ice was measured on that day, the ice layer was located in the middle of the PSC, between 21 and 23 km. The trajectory considered here was started at 20 km, thus at the bottom of the PSC and therefore below the ice layer (Fig. 2). With increasing H$_2$O mixing ratio the T_{NAT} threshold temperature is higher and temperatures can more easily drop below T_{NAT}. However, a slight prolongation of temperatures below T_{NAT} is found only for the temperature range T_1 (Table 1). Although the effect on T_{NAT} seems to be insignificant in this example, the effect on T_{ice} seems to be more significant. Temperatures did not drop below T_{ice} but came very close to the T_{ice} threshold when water vapour mixing ratios were increased. Therefore, another trajectory has been chosen, one where T_{ice} was reached along the trajectory using a water vapour mixing ratio of 5 ppmv (typical water vapour mixing ratio during polar winter). This trajectory is discussed in the following section.

only a few PSCs were detected which were located around Greenland[2].

4.1 Sensitivity studies on single back trajectories

4.1.1 Case 1: sensitivity to H$_2$O enhancements

Figure 2 shows the CALIPSO measurement on 26 February 2011 around 00:04 UTC. A PSC was measured at altitudes between 16 and 24 km (between 76° N, 61° E to 70° N, 49° E). The PSC was located east of Novaya Zemlya and was composed of all kinds of PSC particles but mainly of STS with a thick ice layer in between (Fig. 2). Based on the PSC observed on 26 February 2011 air parcel trajectories were calculated 6 days backwards with the HYSPLIT model. The trajectories were started at 00:00 UTC at 20, 22 and 24 km (started at 71° N, 61° E) and ended at 20 February at 00:00 UTC. During the course of the 6 days the trajectories followed the circular flow within the polar vortex and thus the air masses were transported twice around in the polar regions (see Fig. S3 in the Supplement).

Figure 3 shows the temperature along the trajectory started at 20 km (black line) together with the threshold temperatures for T_{NAT} and T_{ice} (red solid and dashed line, respectively). The threshold temperatures were calculated ac-

4.1.2 Case 2: sensitivity to H$_2$O enhancements and additional cooling

Figure 4 shows the CALIPSO measurement on 23 January 2011. A PSC was measured over Russia at altitudes between 16 and 23 km (80° N, 139° E to 66° N, 105° E). Based on the PSC measured on 23 January 2011, back trajectories were calculated with HYSPLIT 6 days backwards starting at 20:00 UTC at three different altitudes within the PSC, namely at 18, 20 and 22 km (started at 72° N, 113° E). During the course of the 6 days the trajectories followed the circular flow within the polar vortex and thus the air masses were

---

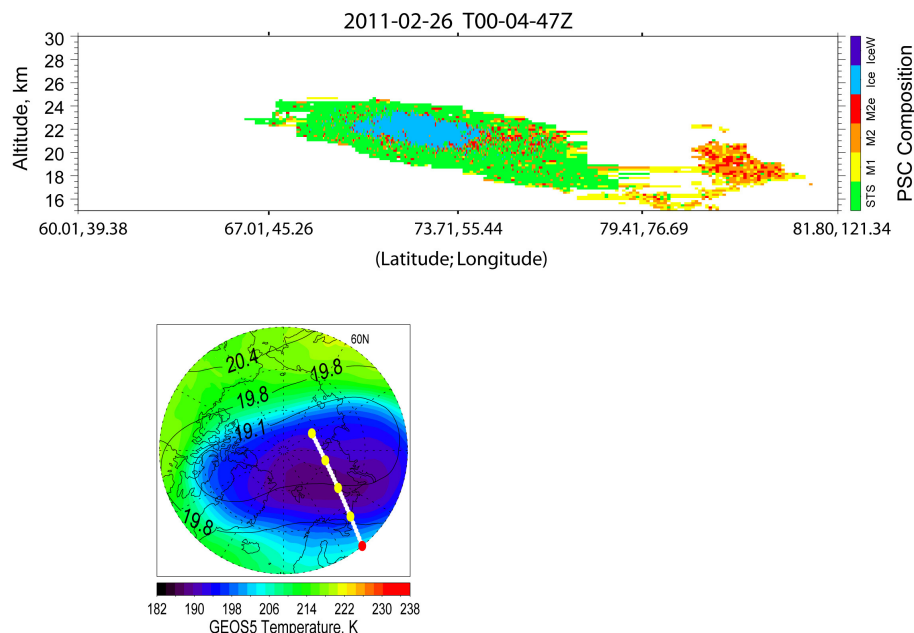[2]Note: no CALIPSO observations are available from 8 to 13 March.

Figure 2. CALIPSO PSC composition for the PSC measured along the orbit track starting at 25 February 2011, 23:56 UTC. Shown is the composition for the measurement on 26 February 2011 at 00:04 UTC and the GEOS-5 temperatures and geopotential height fields (in gpkm) at 30 hPa at 12:00 UTC (bottom). The white line marks the CALIPSO orbit track.

transported twice around in the polar regions (see Fig. S4 in the Supplement). As in the previous example, the PSC was composed of all kinds of PSC particles, but STS, Mix 2 enhanced (liquid/NAT mixture with intermediate NAT number densities of $10^{-3}\,\mathrm{cm}^{-3}$) and some ice in between was dominating (Fig. 4).

Figure 5 shows the temperature along the trajectory (black) that was started at 18 km as well as the threshold temperatures for T_{NAT} and T_{ice} (red solid and dashed line, respectively). As in the case discussed in Sect. 4.1.1, the threshold temperatures were calculated for 5 ppmv (typical water mixing ratio during polar winter (Achtert et al., 2011, and references therein, Khosrawi et al., 2011) and for increased water vapour mixing ratios of 5.5 and 6 ppmv (middle and bottom panel). In this case, the temperatures drop twice below T_{NAT} along the trajectory, at $t = -135$ to $-105\,\mathrm{h}$ (temperature range T_1) and $t = -45$ to $0\,\mathrm{h}$ (temperature range T_2). Temperatures during the second time period with $T_2 < T_{\mathrm{NAT}}$ were colder and even reached T_{ice}. The time periods where temperatures were lower than T_{NAT} are prolonged when the atmospheric water vapour mixing ratio is increased (Table 2). For example, while the T_1 temperatures did not reach below T_{NAT} under normal stratospheric conditions, temperatures reach 15 and 30 h below T_{NAT} with an increase in H$_2$O mixing ratio of 0.5 and 1 ppmv, respectively, thus allowing STS and NAT PSC formation and existence during a longer time period.

The effect becomes even stronger when additionally the temperature is decreased (Fig. 6). Time periods where T_1 or

T_2 are below T_{NAT} and T_{ice} become much longer, as can be seen from Table 2. Further, the effect becomes more pronounced for T_{ice} as can be expected, but there seems to be also an increase in T_2 below T_{NAT} due to strong temperature cooling along the trajectory.

4.2 Sensitivity studies on back trajectory ensemble

The back trajectory ensemble was calculated starting at dates and times when PSCs were measured by CALIPSO during the Arctic winter 2010/11. For each PSC measurement, trajectories were calculated 6 days backward in time at three different altitudes, corresponding to the top, middle and bottom of the cloud. In total 738 trajectories were calculated. During the course of the 6 days the trajectories in general followed the circular flow within the polar vortex and thus the air masses were transported once or several times around in the polar regions. The temperature thresholds for PSC formation encountered along the trajectories derived with HYSPLIT are in good agreement with the corresponding PSC types measured by CALIPSO.

Using the entire trajectory ensemble the total time (sum over all 738 trajectories) where the temperature was below T_{NAT} and T_{ice}, respectively, was estimated applying an H$_2$O mixing ratio of 5 ppmv (same as in Sect. 4.1.1 and 4.1.2, typical water vapour mixing ratio for the Arctic polar lower stratosphere (Achtert et al., 2011, and references therein, Khosrawi et al., 2011) and observed by the satellite instruments considered in this study). This calculation was repeated applying a H$_2$O increase of 0.25–1 ppmv

Table 2. Time periods when T_1 and T_2 are below the NAT and ice threshold temperature along the trajectory. T_{NAT} and T_{ice} were derived for H₂O mixing ratios of 5, 5.5. and 6 ppmv for the back trajectory started on 23 January 2011 at 20:00 UTC (Case 2). Water vapour increases (Case 2a) as well as an additional temperature cooling by 1 K (Case 2b) are considered.

H₂O (ppmv)	Case 2a			Case 2b		
	$T_1 < T_{NAT}$ (h)	$T_2 < T_{NAT}$ (h)	$T_2 < T_{ice}$ (h)	$T_1 < T_{NAT}$ (h)	$T_2 < T_{NAT}$ (h)	$T_2 < T_{ice}$ (h)
5	10	38	–	45	35	20
5.5	25	41	15	45	42	22
6	30	44	20	> 45	47	25

(ΔH₂O $= 0.25$ ppmv, as in Sect. 4.1.1 and 4.1.2, according to the estimated trends from Rosenlof et al., 2001 and Hurst et al., 2011) as well as a decrease in temperature by 0.5 and 1 K. Additionally, the calculation was repeated for a water vapour decrease of 0.25 ppmv to also investigate what the effect of an opposite change would be, which could result from the natural H₂O variability. To quantify the effect a change in H₂O mixing ratio and a decrease in temperature would have, we calculated the enhancement in time that would result when the temperatures would be exposed accordingly longer to temperatures below T_{NAT} and T_{ice}.

The results of the sensitivity study with the trajectory ensemble are summarised in Figs. 7 and 8 for T_{NAT} and in Figs. 9 and 10 for T_{ice}. In Figs. 7 and 9 the total time the temperature is below T_{NAT} and T_{ice}, respectively, is given while in Figs. 8 and 10 the additional time is given when the temperature would be below T_{NAT} and T_{ice}, respectively, if the H₂O mixing ratio would increase and temperature decrease (see also tables in Supplement). The calculation of extra exposure time to T_{NAT} and T_{ice} was done assuming HNO₃ mixing ratios of 7, 5 and 3 ppmv which corresponds to the conditions in the polar lower stratosphere at the beginning of the winter and later in the winter when HNO₃ has been taken up by the PSCs and HNO₃ has been permanently removed by sedimenting PSC particles (denitrification).

For the reference conditions (normal stratospheric winter conditions, beginning of the winter, thus prevailing gas phase abundances of 5 ppmv H₂O and 7 ppmv HNO₃) temperatures were in total below T_{NAT} for 43 512 h (Fig. 7). Note: total trajectory time is 107 010 h (738 trajectories × 145 h). If HNO₃ decreases during the course of the winter to 5 ppbv the air will be ∼ 3600 h less exposed to temperatures below T_{NAT}. If HNO₃ will further decrease to 3 ppbv the total time will be ∼ 5000 h less than during reference conditions. On the other hand, if in the future H₂O increases and the temperature decreases in the stratosphere, the total time where temperature falls below T_{NAT} will increase independent of the HNO₃ abundance (3, 5 or 7 ppbv) in the stratosphere (Fig. 8). Any H₂O increase of 0.25 ppmv will result in 1500 h more where the temperature along the trajectories will be below T_{NAT}. The effect is much stronger when the temperature is

decreased by 0.5 K. For each 0.5 K cooling the time will be increased by ∼ 4000 h (Fig. 7 and tables in the Supplement).

Temperatures below T_{ice} are rarely reached in the Arctic. However, the Arctic winter 2010/11 was exceptionally cold and temperatures below T_{ice} were reached along several trajectories. Under typical stratospheric conditions (H₂O $= 5$ ppmv) temperatures were below T_{ice} for 571 h (Fig. 9). If the H₂O abundance in the stratosphere is 0.25 ppmv less (thus 4.75 ppmv) than the total time where the temperatures are below T_{ice} decreases to 340 h, 231 h less than under the reference stratospheric conditions (Fig. 10 and the Supplement). If the H₂O mixing ratio increases by 0.25 ppmv, from 5 to 5.25 ppmv, temperatures below T_{ice} would persist 299 h longer than for reference conditions. If water vapour increases further from 5 to 5.5 or 6 ppmv, the time where temperatures are below T_{ice} will increase by 669 and 1728 h, respectively. Thus, the higher the water vapour gets in the stratosphere the stronger the impact of a further increase will be. The same behaviour is found when the temperature in the stratosphere is cooled by 0.5 to 1 K. In the extreme case when H₂O mixing ratios would increase by 1 ppmv and the temperature would decrease by 1 K the total time where temperatures are below T_{ice} would increase from 571 to 6789 h, thus by ∼ 6000 h which corresponds to an enhancement by a factor of 12.

5   Water vapour and temperature variability (2000–2014)

In the previous section we demonstrated that a water vapour increase and temperature decrease would increase the potential for PSC formation. More than a decade ago it was already suggested that a cooling of stratospheric temperatures by 1 K or an increase of 1 ppmv of stratospheric water vapour could promote denitrification (Santee et al., 1995; Tabazadeh et al., 2000). During the two Arctic winters 2009/10 and 2010/11, the strongest denitrification in the recent decade was observed (Khosrawi et al., 2011, 2012).

Here, we investigate the variability of Arctic water vapour and temperature since the new millennium to see if there is a connection to the severe denitrification ob-
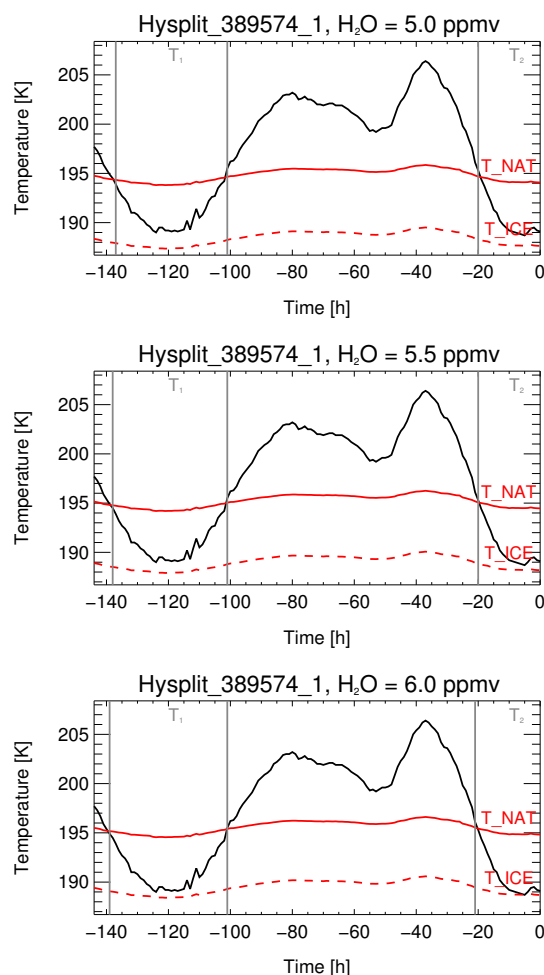
Figure 3. Temperature history of the back trajectory calculated with HYSPLIT based on the PSC measured by CALIPSO on 26 February 2011 (back trajectory started at 20 km at 00:00 UTC). Top: for a typical H_2O mixing ratio of 5 ppmv in the polar lower stratosphere, middle: for an H_2O enhancement of 0.5 ppmv (5.5 ppmv), bottom: for an H_2O enhancement of 1 ppmv (6 ppmv). The NAT existence temperature T_{NAT} and ice formation temperature T_{ice} are given as solid and dashed lines, respectively. Temperatures drop below the NAT formation temperature at time periods $t = -140$ to -100 h and $t = -20$ to 0 h. The temperature ranges during these time periods are denoted by T_1 and T_2, respectively (grey solid lines).

served in the past years. For that we used observations from UARS/HALOE, Odin/SMR, Envisat/MIPAS, SCISAT/ACE-FTS, Envisat/SCIAMACHY and Aura/MLS as well as ERA interim reanalysis data. In a first step these data sets were interpolated onto a regular potential temperature grid with a resolution of 25 K. Temperature and pressure data needed for the conversion from the native vertical coordinate to potential temperature were taken from the individual data sets themselves. Then for every profile the equivalent latitude as function of altitude was derived from ERA interim potential vor-

ticity data. Data within high equivalent latitudes, i.e. between 70 to 90° N, were subsequently binned into monthly and zonally averaged time series. Finally the resulting time series were de-seasonalised to make variability on inter-annual to decadal scales more visible. For a given month a multi-year average was calculated from the individual monthly averages which was then subtracted from the latter. The multi-year averages were based on the entire time period covered by the individual data sets.

Figure 11 shows the de-seasonalised time series for temperature (upper panel) and water vapour (lower panel) covering the time period 2000–2014 averaged over the potential temperature range 475–525 K ($\sim$ 18–22 km). Temperature information is provided by ERA-Interim, Aura/MLS, Envisat/MIPAS and SCISAT/ACE-FTS; for water vapour there is in addition also data from UARS/HALOE and Envisat/SCIAMACHY. In terms of temperature there is a very good agreement among the different data sets. The overall variability is dominated by the winter season. Strong inter-annual variability can be found for this season with pronounced cold and warm events that show absolute anomalies of more than 10 K. For water vapour there is more scatter and less consistency between the individual data sets. Deviations exceed occasionally 0.5 ppmv, which is a typical level of uncertainty of these observations (Hegglin et al., 2013). Unlike temperature the water vapour variability is not as apparently dominated by the winter season. The pronounced events seen in temperature can be still observed in water vapour in an anti-correlated sense, but not as obvious. There are indications of a substantial decrease throughout 2003, however not in all data sets. A similar feature can be observed in 2011. Likewise there are indications of an increase in 2006 and 2007. Overall this demonstrates significant changes over short time periods.

Figure 12 is of the same kind as Fig. 11 however it considers the potential temperature range between 525 and 825 K ($\sim$ 22–28 km). Please note that there are no water vapour data from Envisat/SCIAMACHY available here. For temperature very similar characteristics can be observed as in Fig. 11. This is also true for water vapour. The scatter is somewhat reduced providing a clearer picture on inter-annual to decadal variability. In particular the variations in the aftermath of sudden stratospheric warmings in early 2009 and 2013 are very pronounced here (Labitzke and Kunze, 2009; Orsolini et al., 2010).

Visually, both Figs. 11 and 12 do not indicate any obvious linear changes in temperature or water vapour overall. To investigate this aspect more rigorously we performed separately a regression analysis of the Envisat/MIPAS and the Aura/MLS time series. The selection of these two data sets was based on their extensive and regular observational coverage. The regression model considered an offset, a linear term, periodic variations of 3, 4, 6 and 12 months as well as the QBO in the form of Singapore winds at 50 and
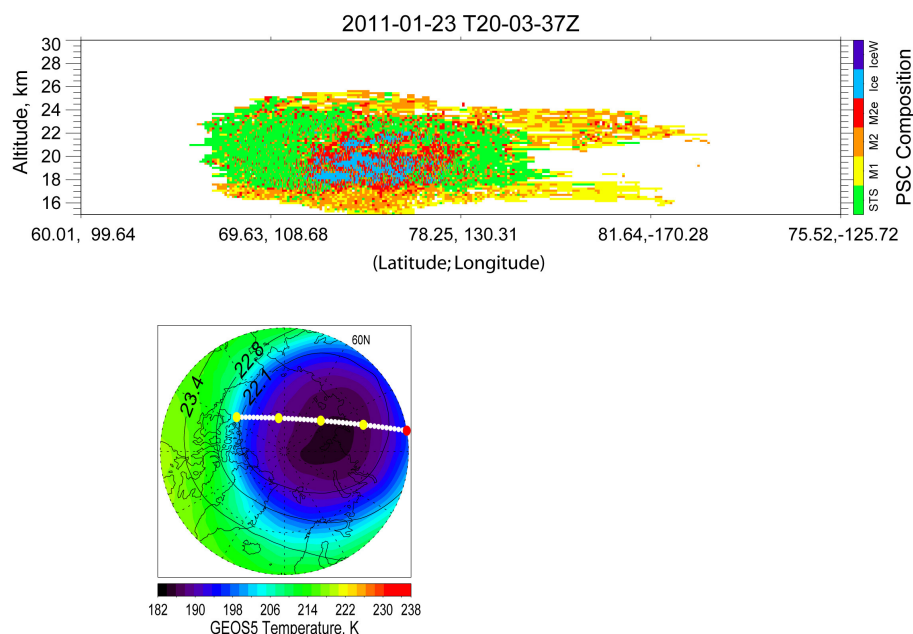
Figure 4. CALIPSO PSC composition for the PSC observation along the orbit track starting at 23 January 2011, 19:52 UTC. Shown is the composition for the measurement on 23 January 2011 at 20:03 UTC (top) and the GEOS-5 temperatures and geopotential height fields (in gpkm) at 30 hPa at 12:00 UT (bottom). The white line marks the CALIPSO orbit track.

30 hPa[3]. In addition the model considered autocorrelation effects and a possible offset between the MIPAS full and reduced resolution data (von Clarmann et al., 2010; Stiller et al., 2012). Figure 13 shows the linear change estimates for water vapour (left panel) and temperature (right panel). Even though the two data sets cover slightly different time periods they indicate largely positive changes in water vapour in the altitude range between 350 and 1000 K potential temperature. The change in absolute terms is typically larger for Aura/MLS than for Envisat/MIPAS, just at the lowest altitudes the behaviour is opposite. For Envisat/MIPAS the linear changes are mostly not significant at the 2σ uncertainty level. The only exception is the altitude range between 375 and 450 K. For Aura/MLS significance is visible at more altitudes, yet there is a number of altitude levels where the changes are close to insignificance. At 1000 K the regression did not converge. The Envisat/MIPAS temperature time series shows largely negative changes that roughly increase with altitude. However none of these changes are significant at the 2σ level. The same is true for the Aura/MLS temperatures, where the trend estimates are more close to zero. Similar results are derived when instead of all seasons only the winter months DJF (the predominant time for PSC formation) is considered (see Supplement).

As noted earlier water vapour and temperature show a clear anti-correlation, e.g. enhanced water vapour mixing ratios occur in cold winters and vice versa. This connection is

---

[3]http://www.geo.fu-berlin.de/met/ag/strat/produkte/qbo/index.html

shown in Fig. 14, that considers as Fig. 11 the altitude range between 475–525 K potential temperature. The individual data points shown here are averages over January, February and March. Both for Envisat/MIPAS and Aura/MLS the correlation is substantial, with correlation coefficients of −0.65 and −0.87, respectively. This clearly indicates a connection between the processes that govern water vapour and temperature in the polar lower stratosphere, as the subsidence inside the polar vortex, sudden stratospheric warmings and radiative cooling. A corresponding figure for the altitude range between 525–825 K is provided in the Supplement. There the correlation is less strong.

Figure 15 shows the altitude time evolution of water vapour in the polar regions derived from Envisat/MIPAS observations for the time period 2002–2012. Differences in the downward transport of water vapour from year to year are clearly visible during the time period 2002–2012. E.g. the transport of high H₂O mixing ratios (e.g. 6 ppmv) reaches much further down into the lower stratosphere (to 20 km and even below) during the Arctic winters as 2006/07, 2007/08 and 2010/11 than in other Arctic winters.

6　Discussion

In the present work we were focusing on the polar regions to understand how water vapour and temperature changes in the lower polar stratosphere affect PSC formation which eventually can also have an impact on denitrification. The influence of water vapour and temperature on PSCs is two-fold.
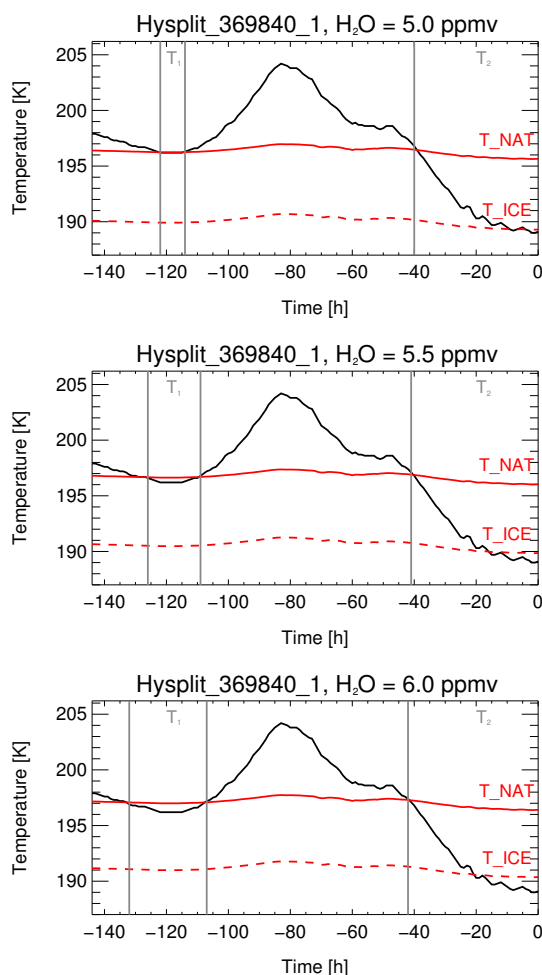
Figure 5. Temperature history of the back trajectory calculated with HYSPLIT based on the PSC measured with CALIPSO on 23 January 2011 (back trajectory started at 18 km at 20:00 UTC). Top: for a typical H$_2$O mixing ratio of 5 ppmv in the polar lower stratosphere, middle: for an H$_2$O enhancement of 0.5 ppmv (5.5 ppmv), bottom: for an H$_2$O enhancement of 1 ppmv (6 ppmv). The NAT existence temperature T_{NAT} and ice formation temperature T_{ice} are given as solid and dashed lines, respectively. Temperatures drop below the NAT formation temperature at time periods $t = -135$ to -105 h and $t = -45$ to 0 h. The temperature ranges during these time periods are denoted by T_1 and T_2, respectively (grey solid lines).

Figure 6. Same as Fig. 5 but with an additional temperature decrease along the back trajectory of 1 K.

There is a background component and on top there is inter-annual variability. The long-term changes of low-latitude water vapour described in the introduction eventually also influence the high latitudes. On the other hand vortex dynamics play an essential role for PSC variations from year to year. Over the time period from 2002 to 2012 Envisat/MIPAS observations indicate a significant change in water vapour only between 375 and 450 K in form of an increase. Aura/MLS observations considering the time period from 2004 to 2014 show positive changes over a wider altitude range, many of
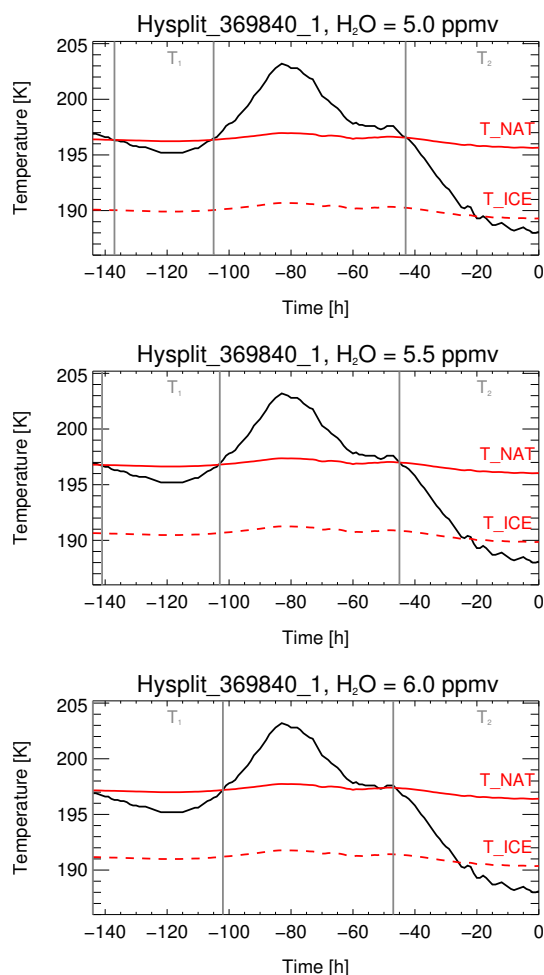
them even significant. Figure 12 indicates that the later start and end of the Aura/MLS measurements relative to the MI-PAS observations could play a decisive role for this difference. In principle an increase is expected. After the long-standing millennium drop a new increase has been observed in the tropics, starting around 2004 to 2005 (Hegglin et al., 2014; Urban et al., 2014). This increase was only interrupted by the 2011 drop that was however much more short-lived than the millennium drop. By early 2014 the volume mixing ratios had more or less recovered (Urban et al., 2014). For the time period since 2002 we cannot find any significant changes in temperature in the altitude range between 350 K and 1000 K potential temperature.

The inter-annual variability component is driven by the vortex-related dynamics and other short-term variations, like QBO and drops in water vapour. During wintertime we found in the satellite data a significant correlation between cold/warm winters and enhanced/reduced water vapour mixing ratios. This correlation indicates a connection between dynamical processes that influence the polar winter dynam-
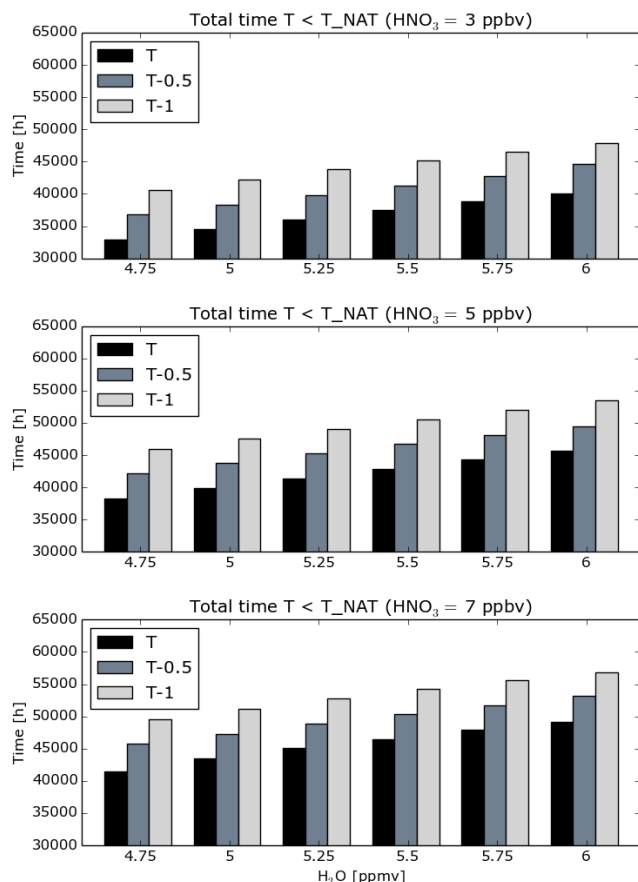
Figure 7. Histograms of the total time where the temperature along the back trajectory is below the NAT existence threshold temperature (sum over all 738 back trajectories) for stratospheric H_2O mixing ratios of 4.75, 5.0, 5.25, 5.5 and 6.0 ppmv. The calculation was performed assuming an HNO_3 mixing ratio of 3 (top), 5 (middle) and 7 ppbv (bottom).

Figure 8. Histogram of increase in time where the temperature along the back trajectory is below the threshold temperature (sum over all 738 back trajectories) for a stratospheric H_2O increase of 0.25, 0.5, 0.75 and 1.0 ppmv, respectively, and for a stratospheric H_2O decrease of 0.25 ppmv. The calculation was performed assuming an HNO_3 mixing ratio of 3 (top), 5 (middle) and 7 ppbv (bottom).

ics. On the one hand there is the subsidence within the polar vortex and its variations. On the other hand there are sudden stratospheric warmings that break up the polar vortex and completely revert the dynamical conditions. During polar winter vigorous descent occurs within the polar vortex, transporting air masses from the upper stratosphere and mesosphere down to the lower stratosphere (Bacmeister et al., 1995). As water vapour typically exhibits a maximum around the stratopause this descent also transports moister air towards the lower stratosphere. Sonkaew et al. (2013) analysed SCIAMACHY data from 2002–2009 and found that the QBO west phase is associated with larger PSC occurrences and stronger chemical ozone destruction than the QBO east phase. Their findings are in agreement with the Holton-Tan mechanism (Holton and Tan, 1980) which relates the QBO west phase to a colder and more stable vortex. During cold Arctic winters, as 2010/2011, the subsidence within the polar vortex is strongly enhanced as shown e.g. by Manney et al.
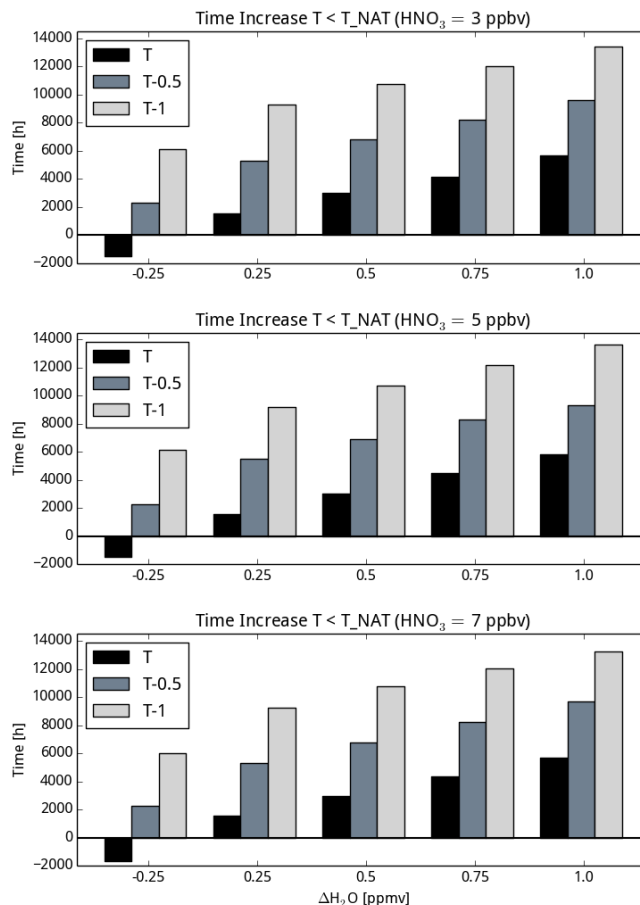
(2008), causing positive water vapour anomalies. This explains already qualitatively the correlation we observed. As an amplifying effect act sudden stratospheric warmings, like in early 2009 or 2013, that led to high positive temperature anomalies and low water vapour. The latter are mainly explained by the poleward transport of dry air once the horizontal mixing barrier in the form of the polar vortex edge is removed.

The signatures of the water vapour drops in 2000 and 2011 are not easily distinguishable in the Arctic. In the altitude range between 475 to 525 K the decrease throughout 2003 may be attributed to the millennium drop. Arctic observations of POAM III indicated the drop already in early 2001 (Randel et al., 2004). This seems to be consistent with studies by Brinkop et al. (2015) that showed a delay of up to 12 months between the drop occurrence in the tropics and at 50° latitude at these low altitudes. The UARS/HALOE
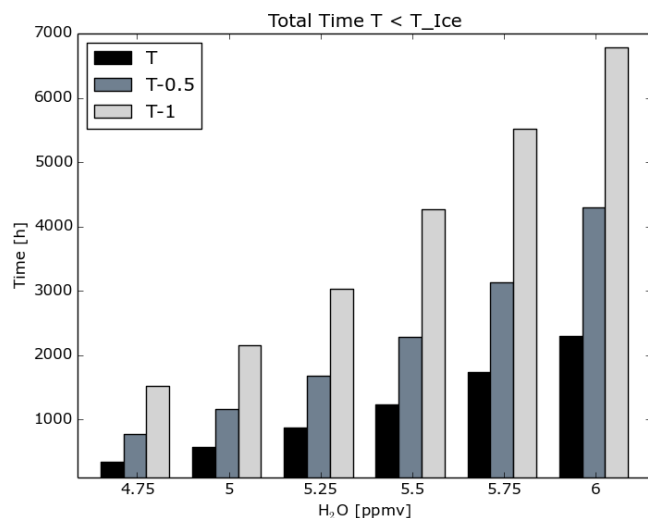
Figure 9. Histogram of total time where the temperature along the back trajectory is below the ice formation threshold temperature (sum over all 738 back trajectories) for a stratospheric H_2O increase of 4.75, 5.0, 5.25, 5.5, 5.75 and 6.0 ppmv.
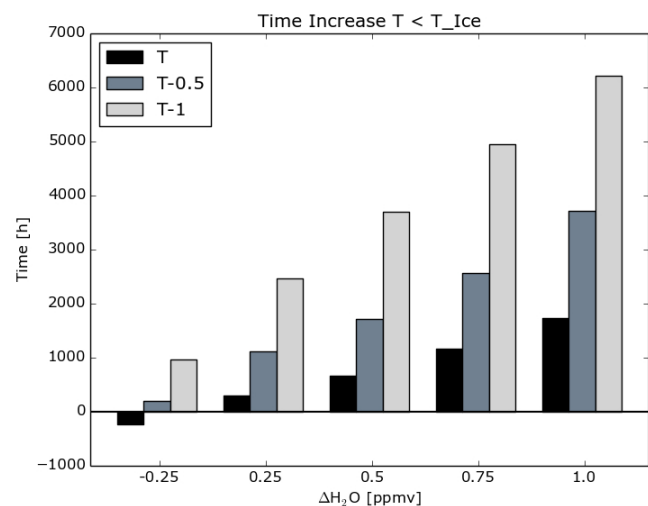

Figure 10. Histogram of increase in time where the temperature along the back trajectory is below the ice formation threshold temperature (sum over all 738 back trajectories) for a stratospheric H_2O increase of 0.25, 0.5, 0.75 and 1.0 ppmv, respectively, and for a stratospheric H_2O decrease of 0.25 ppmv.

observations employed here do not show a clear sign of a decrease in 2001, however admittedly the measurement coverage of this instrument has not been optimal for these high latitudes. The decrease in the Arctic in 2011 may correspond to the drop observed in the tropics. Yet, the length of the decrease is shorter than observed at the low latitudes. Higher up, between 525 K and 825 K potential temperature, a longer delay to the drop occurrence in the tropics can be expected (Stiller et al., 2012; Brinkop et al., 2015). Thus, the decrease observed here in 2002 and 2003 is more likely attributed to

the millennium drop. The decrease in 2011 on the other hand is unlikely to be connected to the tropical event.

Overall, based on the observations since the new millennium we can conclude that such strong denitrification events as in 2010/11 are for the time being driven by inter-annual variability than any changes in water vapour and/or temperature since the millennium.

By performing sensitivity studies we, on one hand, investigate what implications water vapour and temperature changes and/or variability would have on PSC formation and existence. On the other hand this sensitivity study also shows what implications uncertainties in water vapour from measurements and temperature measurements and/or reanalyses would have on Arctic studies. Gravity waves can affect PSC occurrence and composition in the Arctic and Antarctic McDonald et al. (2009); Alexander et al. (2011, 2013). Temperature perturbations that are caused by gravity waves are usually not represented in meteorological analyses. Further, meteorological analyses tend to have cold or warm biases as was shown by e.g. Manney et al. (1996). PSC formation and existence is quite sensitive to temperature and water vapour changes as well as uncertainties of these. An increase of e.g. 1 ppmv in water vapour and a decrease of 1 K in temperature would significantly alter the estimates of PSC volume and area (V_{PSC} and A_{PSC}, respectively) and thus would affect the estimates on e.g. ozone loss and chlorine activation (Manney et al., 2003). However, irrespective of if there is a cold or warm bias in the trajectory temperature or in the water vapour mixing ratio in the stratosphere, an increase in water vapour mixing ratios or a cooling of temperature will definitely result in a prolongation of the potential for PSC existence as shown in our sensitivity study.

Our sensitivity study was performed on the basis of the 2010/11 winter, which was the coldest Arctic winter in the recent decade. The anomalously strong polar vortex and the atypically long cold period that persisted from mid-December to mid-March led to extensive PSC formation. PSCs were observed by CALIPSO over 47 days during the Arctic winter 2010/11. During the Arctic winter 2009/10, a cold period extended over 4 weeks, from mid-December to mid-January, and PSCs were only observed on 26 days. Thus, if this study would have been performed on the basis of another (warmer) winter less PSC observations would have been served as a basis for the trajectory calculations and thus as a basis for the statistic. As a consequence the total times where the temperature was below T_{NAT} or T_{ice}, respectively, would have been shorter as for the Arctic winter 2010/11. However, the resulting increase in time due to a decrease in temperature and an increase in water vapour can be expected to be similar, thus as dramatic as for the 2010/11 winter.

As shown in this study, increases in stratospheric water vapour as well as decreases in stratospheric temperature can prolong PSC formation and existence. An increase of water vapour of 1 ppmv and a decrease of temperature of 1 K increased the times where the temperature is below T_{NAT} by
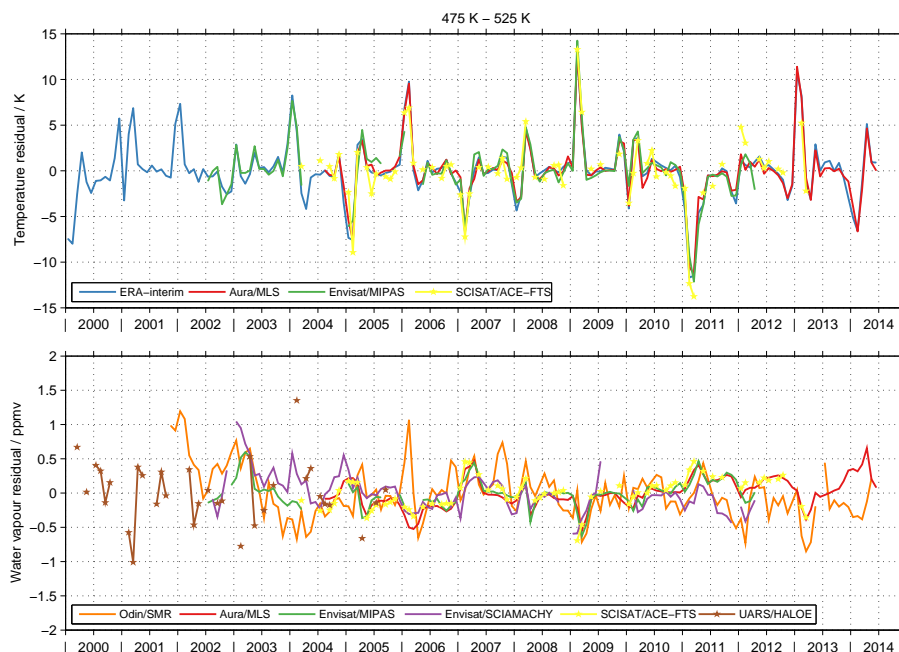
Figure 11. Anomaly of the monthly mean temperature (top) and water vapour for the polar regions at equivalent latitudes (70 to 90° N). The data were averaged within the potential temperature layers 475–525 K (18–22 km). Top: temperature from ERA-interim (blue), Aura/MLS (red), Envisat/MIPAS (green) and SCISAT/ACE-FTS (orange). Bottom: water vapour derived from Odin/SMR at 544 GHz band (orange), Aura/MLS (red), Envisat/MIPAS (green), Envisat/SCIAMACHY (purple), SCISAT/ACE-FTS (yellow) and UARS/HALOE (brown).
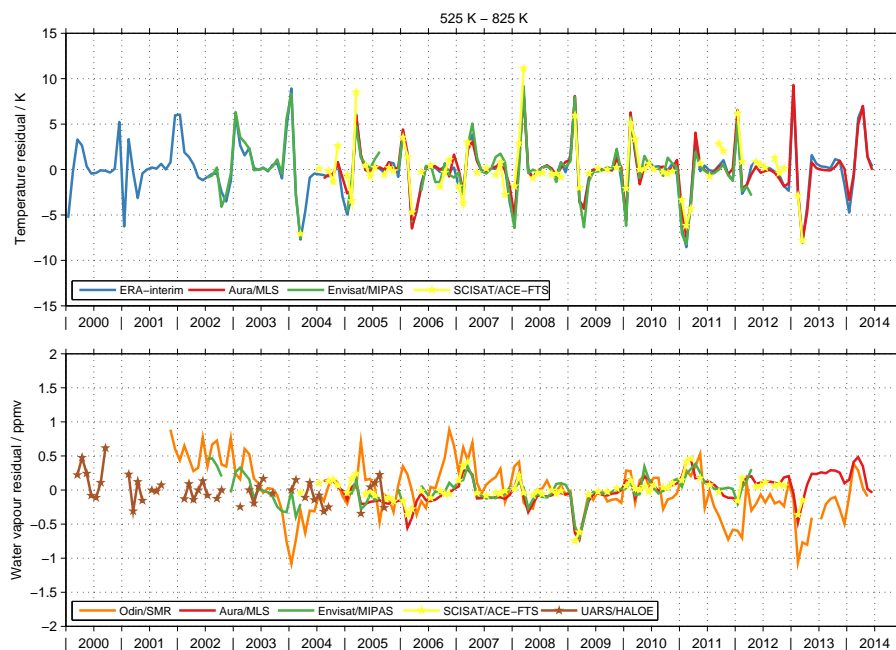
Figure 12. Same as Fig. 2, but for 525–825 K.

38 %. A much stronger increase in time was found for ice. The increase in time where temperatures were below T_{ice} were enhanced by a factor of 12 for an increase of H$_2$O by 1 ppmv and a temperature decrease of 1 K. Generally, tem-

peratures sufficiently low for ice formation are rarely reached in the Arctic. Therefore, this strong increase in time where temperatures would be below T_{ice} would mainly be of importance for very cold, extreme Arctic winters as e.g. the Arctic
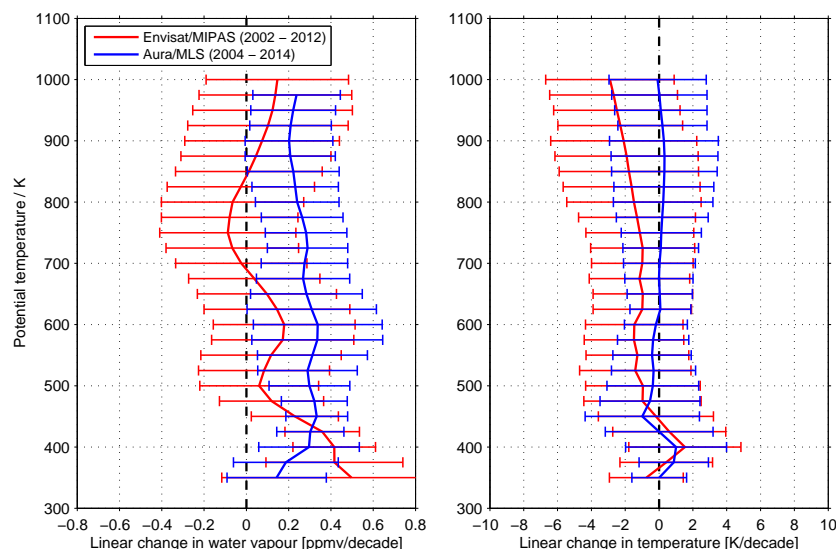
Figure 13. Linear change in water vapour (left) and temperature (right) vs. potential temperature derived from Envisat/MIPAS (2002–2012) and Aura/MLS (2004–2014). For the linear change in water vapour derived from Envisat/MIPAS an offset of 0.1 ppmv between the two measurement periods has been considered. As error bars the 2σ uncertainty is given.
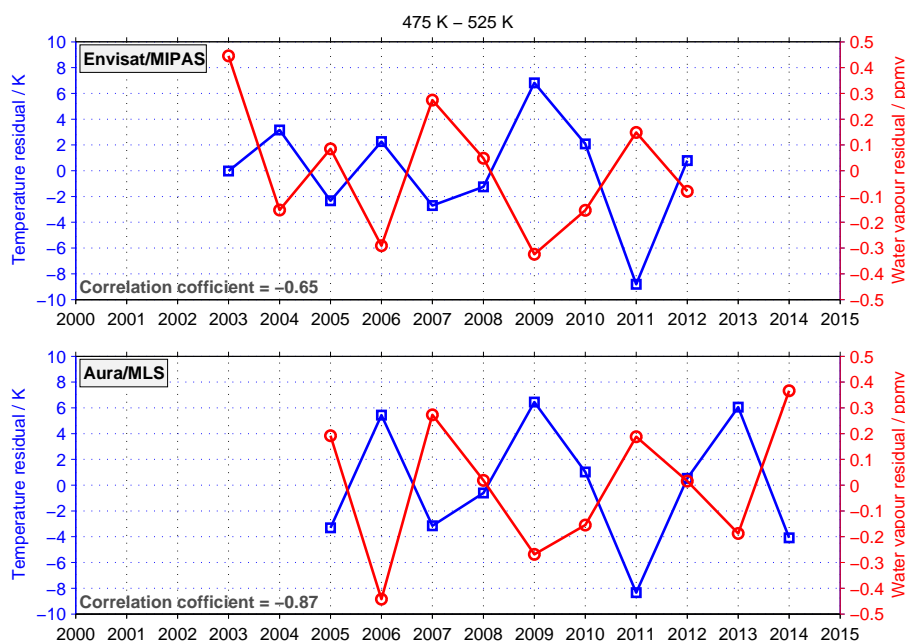

Figure 14. Correlation of temperature (blue) and water vapour (red) anomaly derived from Envisat/MIPAS (top) and Aura/MLS (bottom) for potential temperature range 475–525 K (3 month average consisting of the months January, February and March; MIPAS: 2002–2012, MLS: 2005–2014).

winter 2010/11. However, if cold Arctic winters will become colder in the future as suggested by Rex et al. (2004, 2006), ice formation will also become more common in the Arctic. Thus, changes in stratospheric H$_2$O mixing ratio and temperature can significantly alter PSC formation and existence and thus the chemistry of the polar stratosphere, as e.g. increasing denitrification and thus ozone loss.

7 Conclusions

The Arctic winter 2010/11 was one of the coldest in the last 2 decades. The 2010/11 winter was characterised by an anomalously strong vortex with an atypically long cold period that was persistent from mid-December to mid-March. During the Arctic winter 2010/11 the strongest denitrification
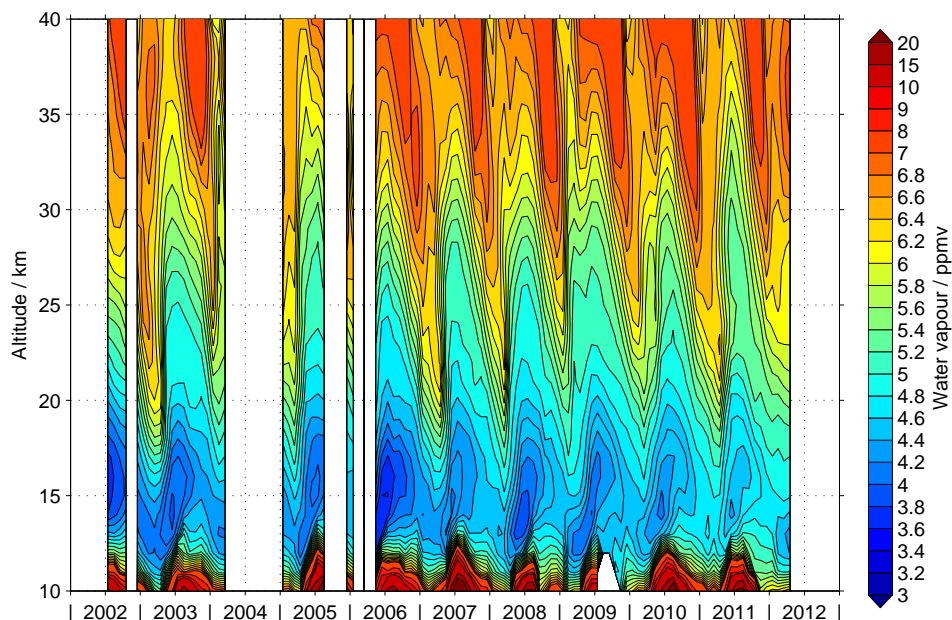
Figure 15. Altitude-time evolution of water vapour in the polar regions (70–90° N) derived from Envisat/MIPAS observation for the time period 2002–2012.

during the recent decade was observed. More than a decade ago it was already suggested that a cooling of stratospheric temperatures by 1 K or an increase of 1 ppmv of stratospheric water vapour could promote denitrification, the removal of HNO_3 by sedimenting PSC particles.

Based on the 2010/11 winter a sensitivity study was performed to investigate how a change of up to 1 ppmv in water vapour and temperature decrease of up to 1 K (due to a trend or variability) would affect PSC formation and occurrence. Air parcel trajectories were calculated 6 days backward according to PSC observations by CALIPSO. In total, 738 trajectories were calculated. On the basis of this trajectory ensemble the increase in time the air parcels would be exposed to temperatures below T_{NAT} or T_{ice} along the trajectories was calculated. Measurements from several different satellites derived for the 15-year period 2000–2014 were used together with temperatures from ECMWF to investigate water vapour trends and variability in the polar stratosphere. So far trend studies on stratospheric water vapour have focused on the tropics and mid-latitudes. Here, for the first time such an analysis has been performed for the polar stratosphere.

Our sensitivity studies based on air parcel trajectories confirm that PSC formation is quite sensitive to water vapour and temperature changes. Increased H_2O (and further cooling of the stratosphere) would increase the potential for PSC formation and prolong PSC existence and thus the chemistry of the polar stratosphere, as e.g. increasing denitrification and thus ozone loss. On the other hand an increase in temperature and a decrease in water vapour will reduce PSC formation and existence. From the Envisat/MIPAS

(2002–2012) and Aura/MLS (2004–2014) observations we derive predominantly positive changes in the altitude range between 350 to 1000 K potential temperature. Those from Envisat/MIPAS observations are largely insignificant, while those from Aura/MLS are mostly significant. For the temperature neither of the two instruments indicate any significant changes. Given the strong inter-annual variation we observed in water vapour and particular temperature the severe denitrification observed in 2010/11 cannot be directly related to any changes in water vapour and/or temperature since the millenium. However, we found from the satellite observations that cold winters coincide with high water vapour mixing ratios, as e.g. for the winters 2006/07, 2007/08 and 2010/11. This correlation is quite significant in the lower stratosphere at 475–525 K and indicates a connection between dynamical and radiative processes that govern water vapour and temperature in the Arctic lower stratosphere.

Dedication to Jo Urban

This work is dedicated to our highly valued colleague Jo Urban who passed away much too early. Without his devoted work on the Odin/SMR data processing over many years this work would not have been possible. In particular the retrieval of water vapour from the SMR observations and the combination of these data with other data sets to understand the long-term development of this trace constituent comprised a large part his life's work. With his death, we lost not only a treasured colleague and friend, but also a leading expert in the microwave and sub-millimetre observation community.

The Supplement related to this article is available online at doi:10.5194/acp-16-101-2016-supplement.

Edited by: C. von Savigny

References

Achtert, P., Khosrawi, F., Blum, U., and Fricke, K.-H.: Investigation of polar stratospheric clouds in January 2008 by means of ground-based and space-borne lidar measurements and microphysical box model simulations, J. Geophys. Res., 116, D07201, doi:10.1029/2010JD014803, 2011.

Alexander, S. P., Klekociuk, A. R., Pitts, M. C., McDonald, A. J., and Arevalo-Torres, A.: The effect of orographic gravity waves on Antarctic polar stratospheric cloud occurrence and composition, J. Geophys. Res., 116, D06109, doi:10.1029/2010JD015184, 2011.

Alexander, S. P., Klekociuk, A. R., McDonald, A. J., and Pitts, M. C.: Quantifying the role of orographic waves on polar stratospheric cloud occurrence in the Antarctic and the Arctic, J. Geophys. Res., 118, 11493–11507, doi:10.1002/2013JD020122, 2013.

Arnone, E., Castelli, E., Papandrea, E., Carlotti, M., and Dinelli, B. M.: Extreme ozone depletion in the 2010–2011 Arctic winter stratosphere as observed by MIPAS/ENVISAT using a 2-D tomographic approach, Atmos. Chem. Phys., 12, 9149–9165, doi:10.5194/acp-12-9149-2012, 2012.

Austin, J., Butchart, N., and Shine, K. P.: Possibility of an Arctic ozone hole in a doubled-CO$_2$ climate, Nature, 360, 221–225, 1992.

Bacmeister, J. T., Schoeberl, M. R., Summers, M. E., Rosenfield, K., and Zhu, X.: Descent of long-lived trace gases in the winter polar vortex, J. Geophys. Res., 100, 11669–11684, doi:10.1029/1995JD02958, 1995.

Bernath, P. F., McElroy, C. T., Abrams, M. C., Boone, C. D., Butler, M., Camy-Peyret, C., Carleer, M., Clerbaux, C., Coheur, P.-F., Colin, R., DeCola, P., DeMaziére, M., Drummond, J. R., Dufour, D., Evans, W. F. J., Fast, H., Fussen, D., Gilbert, K., Jennings, D. E., Llewellyn, E. J., Lowe, R. P., Mahieu, E., McConnell, J. C., McHugh, M., McLeod, S. D., Michaud, R., Midwinter, C., Nassar, R., Nichitiu, F., Nowlan, C., Rinsland, C. P., Rochon, Y. J., Rowlands, N., Semeniuk, K., Simon, P., Skelton, R., Sloan, J. J., Soucy, M.-A., Strong, K., Tremblay, P., Turnbull, D., Walker, K. A., Walkty, I., Wardle, D. A., Wehrle, V., Zander, R., and Zou, J.: Atmospheric Chemistry Experiment (ACE): mission overview, Geophys. Res. Lett., 32, L15S01, doi:10.1029/2005GL022368, 2005.

Bogdan, A., Molina, M. J., Kulmala, M., MacKenzie, A. R., and Laaksonen, A.: Study of finely devided aqueous systems as an aid to understanding the formation mechanism of polar stratospheric clouds: case of HNO$_3$/H$_2$O and H$_2$SO$_4$/H$_2$O system, J. Geophys. Res., 108, 4302, doi:10.1029/2002JD002605, 2003.

Boone, C. D., Nassar, R., Walker, K. A., Rochon, Y., McLeod, S. D., Rinsland, C. P., and Bernath, P. F.: Retrievals for the atmospheric chemistry experiment Fourier transform spectrometer, Appl. Optics, 44, 7218–7231, 2005.

Bovensmann, H., Burrows, J. P., Buchwitz, M., Frerick, J., Noël, S., Rozanov, V. V., Chance, K. V., and Goede, A. P. H.: SCIAMACHY: mission objectives and measurement modes, J. Atmos. Sci., 56, 127–150, 1999.

Brinkop, S., Dameris, M., Jöckel, P., Garny, H., Lossow, S., and Stiller, G.: The millennium water vapour drop in chemistry-climate model simulations, Atmos. Chem. Phys. Discuss., 15, 24909–24953, doi:10.5194/acpd-15-24909-2015, 2015.

Burrows, J. P., Hölzle, E., Goede, A. P. H., Visser, H., and Fricke, W.: SCIAMACHY – scanning imaging absorption spectrometer for atmospheric chartography, Acta Astronaut., 35, 445–451, 1995.

Carslaw, K. S., Luo, B. P., Clegg, S. L., Peter, T., Brimblecombe, P., and Crutzen, P. J.: Stratospheric aerosol growth and HNO$_3$ gas phase depletion from coupled HNO$_3$ and water uptake by liquid particles, Geophys. Res. Lett., 21, 2479–2482, 1994.

Dessler, A. E., Schoeberl, M. R., Wang, T., Davis, S. M., Rosenlof, K. H., and Vernier, J.-P.: Variations of stratospheric water vapour over the past three decades, J. Geophys. Res., 119, 12588–12598, doi:10.1002/2014JD021712, 2014.

Engel, I., Luo, B. P., Khaykin, S. M., Wienhold, F. G., Vömel, H., Kivi, R., Hoyle, C. R., Grooß, J.-U., Pitts, M. C., and Peter, T.:

Arctic stratospheric dehydration – Part 2: Microphysical modeling, Atmos. Chem. Phys., 14, 3231–3246, doi:10.5194/acp-14-3231-2014, 2014.

Eyring, V., Cionni, I., Lamarque, J. F., Akiyoshi, H., Bodeker, G. E., Charlton-Perez, A. J., Frith, S. M., Gettelman, A., Kinnison, D. E., Nakamura, T., Oman, L. D., Pawson, S., and Yamashita, Y.: Sensitivity of 21st century stratospheric ozone to greenhouse gas scenarios, Geophys. Res. Lett., 37, L16807, doi:10.1029/2010GL044443, 2010.

Fischer, H. and Oelhaf, H.: Remote sensing of vertical profiles of atmospheric trace constituents with MIPAS limb-emission spectrometers, Appl. Optics, 35, 2787–2796, 1996.

Fischer, H., Birk, M., Blom, C., Carli, B., Carlotti, M., von Clarmann, T., Delbouille, L., Dudhia, A., Ehhalt, D., Endemann, M., Flaud, J. M., Gessner, R., Kleinert, A., Koopman, R., Langen, J., López-Puertas, M., Mosner, P., Nett, H., Oelhaf, H., Perron, G., Remedios, J., Ridolfi, M., Stiller, G., and Zander, R.: MIPAS: an instrument for atmospheric and climate research, Atmos. Chem. Phys., 8, 2151–2188, doi:10.5194/acp-8-2151-2008, 2008.

Frisk, U., Gastrom, M., Ala-Laurinaho, J., Andersson, S., Berges, J. C., Chabaud, J. P., Dahlgren, M., Emrich, A., Florin, G., Fredrixon, M., Gaier, T., Haas, R., Hjalmarsson, T. H. A., Jakobsson, B., Jukkala, P., Kildal, P. S., Kollberg, E., Lecacheux, J. L. A., Lehikoinen, P., Lehto, A., Mallat, J., Marty, C., Michet, D., Narbonne, J., Nexon, M., Olberg, M., Olofsson, A. O. H., Olofsson, G., Origne, A., Petersson, M., Piirone, P., Pouliquen, D., Ristorcelli, I., Rosolen, C., Rouaix, G., Raisanen, A. V., Serra, G., Sjoberg, F., Stenmark, L., Torchinsky, S., Tuovinen, J., Ullberg, C., Vinterhav, E., Wadefalk, N., Zirath, H., Zimmermann, P., and Zimmermann, R.: The Odin satellite: I. Radiometer design and test, Astron. Astrophys., 403, 27–34, 2003.

Fueglistaler, S., Buss, S., Luo, B. P., Wernli, H., Flentje, H., Hostetler, C. A., Poole, L. R., Carslaw, K. S., and Peter, Th.: Detailed modeling of mountain wave PSCs, Atmos. Chem. Phys., 3, 697–712, doi:10.5194/acp-3-697-2003, 2003.

Gettelman, A., Hegglin, M. I., Son, S., Kim, J., Fujiwara, M., Birner, T., Kremser, S., Rex, M., Anel, J. A., Austin, H. A. J., Bekki, S., Braesicke, P., Brühl, C., Butchart, N., Chipperfield, M., Dameris, M., Dhomse, S., Garny, H., Hardiman, S. C., Jöckel, P., Kinnison, D. E., Lamarque, J. F., Mancini, E., Marchand, M., Michou, M., Morgenstern, O., Pawson, S., Pitari, G., Plummer, D., Pyle, J. A., Rozanov, E., Scinocca, J., Shepherd, T. G., Shibata, K., Smale, D., Teyssèdre, H., and Tian, W.: Multimodel assessment of the upper troposphere and lower stratosphere: tropics and global trends, J. Geophys. Res., 115, D00M08, doi:10.1029/2009JD013638, 2010.

Gottwald, M., Bovensmann, H., Lichtenberg, G., Noel, S., von Bargen, A., Slijkhuis, S., Piters, A., Hoogeveen, R., von Savigny, C., Buchwitz, M., Kokhanovsky, A., Richter, A., Rozanov, A., Holzer-Popp, T., Bramstedt, K., Lambert, J.-C., Skupin, J., Wittrock, F., Schrijver, H., and Burrows, J.: SCIAMACHY, Monitoring the Changing Earth's Atmosphere, Springer, Dordrecht, Heidelberg, London, New York, 2006.

Hanson, D. R. and Mauersberger, K.: Laboratory studies of the nitric acid trihydrate: implications for the south polar stratosphere, Geophys. Res. Lett., 15, 855–858, 1988.

Harris, J. E., Russell, J. M., Tuck, A. F., Gordely, L. L., Purcell, P., Stone, K., Bevilacqua, R. M., Gunson, M., Nedoluha, G.,

and Traub, W. A.: Validation of measurements of water vapour from the Halogen Occultation Experiment (HALOE), J. Geophys. Res., 101, 10205–10216, 1996.

Hegglin, M. I., Tegtmeier, S., Anderson, J., Froidevaux, L., Fuller, R., Funke, B., Jones, A., Lingenfelser, G., Lumpe, J., Pendlebury, D., Remsberg, E., Rozanov, A., Toohey, M., Urban, J., von Clarmann, T., Walker, K. A., Wang, R., and Weigel, K.: SPARC data initiative: comparison of water vapor climatologies from international satellite limb sounders, J. Geophys. Res., 118, 11824–11846, doi:10.1002/jgrd.50752, 2013.

Hegglin, M. I., Plummer, D. A., Shepherd, T. G., Scinocca, J. F., Anderson, J., Froidevaux, L., Funke, B., Hurst, D., Rozanov, A., Urban, J., von Clarmann, T., Walker, K. A., Wang, H. J., Tegtmeier, S., and Weigel, K.: Vertical structure of stratospheric water vapour trends derived from merged satellite data, Nat. Geosci., 7, 768–776, doi:10.1038/ngeo2236, 2014.

Holton, J. R. and Tan, H. C.: The influence of the equatorial Quasi-Biennial Oscillation on the global circulation at 50 mb, J. Atmos. Sci., 37, 2200–2208, 1980.

Hommel, R., Eichmann, K.-U., Aschmann, J., Bramstedt, K., Weber, M., von Savigny, C., Richter, A., Rozanov, A., Wittrock, F., Khosrawi, F., Bauer, R., and Burrows, J. P.: Chemical ozone loss and ozone mini-hole event during the Arctic winter 2010/2011 as observed by SCIAMACHY and GOME-2, Atmos. Chem. Phys., 14, 3247–3276, doi:10.5194/acp-14-3247-2014, 2014.

Höpfner, M., Larsen, N., Spang, R., Luo, B. P., Ma, J., Svendsen, S. H., Eckermann, S. D., Knudsen, B., Massoli, P., Cairo, F., Stiller, G., v. Clarmann, T., and Fischer, H.: MIPAS detects Antarctic stratospheric belt of NAT PSCs caused by mountain waves, Atmos. Chem. Phys., 6, 1221–1230, doi:10.5194/acp-6-1221-2006, 2006.

Höpfner, M., Pitts, M. C., and Poole, L. R.: Comparison between CALIPSO and MIPAS observations of polar stratospheric clouds, J. Geophys. Res., 114, D00H05, doi:10.1029/2009JD012114, 2009.

Hoyle, C. R., Engel, I., Luo, B. P., Pitts, M. C., Poole, L. R., Grooß, J.-U., and Peter, T.: Heterogeneous formation of polar stratospheric clouds – Part 1: Nucleation of nitric acid trihydrate (NAT), Atmos. Chem. Phys., 13, 9577–9595, doi:10.5194/acp-13-9577-2013, 2013.

Hurst, D. F., Oltmans, S. J., Vömel, H., Rosenlof, K. H., Davies, S. M., Ray, E. A., Hall, E. G., and Jordan, A. F.: Stratospheric water vapour trends over Boulder, Colorado: analysis of 30 year Boulder record, J. Geophys. Res., 116, D02306, doi:10.1029/2010JD015065, 2011.

Hurst, D. F., Lambert, A., Read, W. G., Davis, S. M., Rosenlof, K. H., Hall, E. G., Jordan, A. F., and Oltmans, S. J.: Validation of aura microwave limb sounder stratospheric water vapor measurements by the NOAA frost point hygrometer, J. Geophys. Res., 119, 1612–1625, doi:10.1002/2013JD020757, 2014.

Hurwitz, M. M., Newman, P. A., and Garfinkel, C. I.: The Arctic vortex in March 2011: a dynamical perspective, Atmos. Chem. Phys., 11, 11447–11453, doi:10.5194/acp-11-11447-2011, 2011.

Khosrawi, F., Urban, J., Pitts, M. C., Voelger, P., Achtert, P., Kaphlanov, M., Santee, M. L., Manney, G. L., Murtagh, D., and Fricke, K.-H.: Denitrification and polar stratospheric cloud formation during the Arctic winter 2009/2010, Atmos. Chem. Phys., 11, 8471–8487, doi:10.5194/acp-11-8471-2011, 2011.

Khosrawi, F., Urban, J., Pitts, M. C., Voelger, P., Achtert, P., Santee, M. L., Manney, G. L., and Murtagh, D.: Denitrification and polar stratospheric cloud formation during the Arctic winter 2009/2010 and 2010/2011 in comparison, in: Proceedings of the ESA Atmospheric Science Conference: Advances in Atmospheric Science and Appplication, 18–22 June 2012, Brugge, Belgium, edited by: Ouwehand, L., ESA-SP-708, Eur. Space Agency Spec. Publ., ISBN/ISSN:978-92-9092-272-8, 2012.

Koop, T., Biermann, U. M., Raber, W., Luo, B. P., Crutzen, P. J., and Peter, T.: Do stratospheric aerosol droplets freeze above the ice frost point?, Geophys. Res. Lett., 22, 917–920, 1995.

Kuttippurath, J., Godin-Beekmann, S., Lefèvre, F., Nikulin, G., Santee, M. L., and Froidevaux, L.: Record-breaking ozone loss in the Arctic winter 2010/2011: comparison with 1996/1997, Atmos. Chem. Phys., 12, 7073–7085, doi:10.5194/acp-12-7073-2012, 2012.

Labitzke, K. and Kunze, M.: On the remarkable Arctic winter in 2008/2009, J. Geophys. Res., 114, D00I02, doi:10.1029/2009JD012273, 2009.

Lambert, A., Read, W. G., Livesey, N. J., Santee, M. L., Manney, G. L., Froidevaux, L., Wu, D. L., Schwartz, M. J., Pumphrey, H. C., Jimenez, C., Nedoluha, G. E., Cofield, R. E., Cuddy, D. T., Daffer, W. H., Drouin, B. J., Fuller, R. A., Jarnot, R. F., Knosp, B. W., Pickett, H. M., Perun, V. S., Snyder, W. V., Stek, P. C., Thurstans, R. P., Wagner, P. A., Waters, J. W., Jucks, K. W., Toon, G. C., Stachnik, R. A., Bernath, P. F., Boone, C. D., Walker, K. A., Urban, J., Murtagh, D., Elkins, J. W., and Atlas, E.: Validation of the aura microwave limb sounder middle atmosphere water vapor and nitrous oxide measurements, J. Geophys. Res., 112, D24S36, doi:10.1029/2007JD008724, 2007.

Llewellyn, E. J., Lloyd, N. D., Degenstein, D. A., Gattinger, R. L., Petelina, S. V., Bourassa, A. E., Wiensz, J. T., Ivanov, E. V., Dade, I. C. M., Solheim, B. H., Connell, J. C. M., Haley, J. C., von Savigny, C., Sioris, C. E., McLinden, C. A., Griffioen, E., Kaminski, J., Evans, W. F., Puckrin, E., Strong, K., Wehrle, V., Hum, R. H., Kendall, D. J. W., Matsushita, J., Murtagh, D. P., Brohede, S., Stegman, J., Witt, G., Barnes, G., Payne, W. F., Piché, L., Smith, K., Warshaw, G., Deslauniers, D.-L., Marchand, P., Richardson, E. H., King, R. A., Wevers, I., McCreath, W., Kyrölä, E., Oikarinen, L., Leppelmeier, G. W., Auvinen, H., Mégie, G., Hauchecorne, A., Lefèvre, F., de La Nöe, J., Ricaud, P., Frisk, U., Sjoberg, F., von Schéele, F., and Nordh, L.: The OSIRIS instrument on the Odin spacecraft, Can. J. Phys., 82, 411–422, 2004.

Luo, B. P., Voigt, C., Fueglistaler, S., and Peter, T.: Extreme NAT supersaturations in mountain wave ice PSCs: a clue to NAT formation, J. Geophys. Res., 108, 4441, doi:10.1029/2002JD003104, 2003.

Manney, G. L., Swinbank, R., Massie, S. T. S., Gelman, M. E., Miller, A. J., Nagatani, R., ONeill, A., and Zurek, R. W.: Comparison of UK Meteorological Office and US National Meteorological Center stratospheric analyses during northern and southern winter, J. Geophys. Res., 101, 10311–10334, doi:10.1029/95JD03350, 1996.

Manney, G. L., Sabutis, J. L., Pawson, S., Santee, M. L., Naujokat, B., Swinbank, R., Gelman, M. E., and Ebisuzaki, W.: Lower stratospheric temperature differences between meteorological analyses in two cold winters and their impact on polar processing studies, J. Geophys. Res., 108, 8328, doi:10.1029/2001JD001149, 2003.

Manney, G. L., Daffer, W. H., Strawbridge, K. B., Walker, K. A., Boone, C. D., Bernath, P. F., Kerzenmacher, T., Schwartz, M. J., Strong, K., Sica, R. J., Krüger, K., Pumphrey, H. C., Lambert, A., Santee, M. L., Livesey, N. J., Remsberg, E. E., Mlynczak, M. G., and Russell III, J. R.: The high Arctic in extreme winters: vortex, temperature, and MLS and ACE-FTS trace gas evolution, Atmos. Chem. Phys., 8, 505–522, doi:10.5194/acp-8-505-2008, 2008.

Manney, G. L., Santee, L., M., Rex, M., Livesey, N. L., Pitts, M. C., Veefkind, P., Nash, E. R., Woltmann, I., Lehmann, R., Froidevaux, L., Poole, L. R., Schoeberl, M. R., Haffner, D. P., Davies, J., Dorokhov, V., Gernandt, H., Johnson, B., Kivi, R., Kyrö, E., Larsen, N., Levelt, P. F., Makshtas, A., McElroy, C. T., Nakajima, H., Concepcion Parrondo, M., Tarasick, D. W., von der Gathen, P., Walker, K. A., and Zinoviev, N. S.: Unprecedented Arctic ozone loss in 2011, Nature, 478, 469–475, doi:10.1038/nature10556, 2011.

Marti, J. and Mauersberger, K.: A survey and new measurements of ice vapor pressure temperatures between 170 and 250 K, Geophys. Res. Lett., 20, 363–366, 1993.

McDonald, A. J., George, S. E., and Woollands, R. M.: Can gravity waves significantly impact PSC occurrence in the Antarctic?, Atmos. Chem. Phys., 9, 8825–8840, doi:10.5194/acp-9-8825-2009, 2009.

Milz, M., Clarmann, T. v., Bernath, P., Boone, C., Buehler, S. A., Chauhan, S., Deuber, B., Feist, D. G., Funke, B., Glatthor, N., Grabowski, U., Griesfeller, A., Haefele, A., Höpfner, M., Kämpfer, N., Kellmann, S., Linden, A., Müller, S., Nakajima, H., Oelhaf, H., Remsberg, E., Rohs, S., Russell III, J. M., Schiller, C., Stiller, G. P., Sugita, T., Tanaka, T., Vömel, H., Walker, K., Wetzel, G., Yokota, T., Yushkov, V., and Zhang, G.: Validation of water vapour profiles (version 13) retrieved by the IMK/IAA scientific retrieval processor based on full resolution spectra measured by MIPAS on board Envisat, Atmos. Meas. Tech., 2, 379–399, doi:10.5194/amt-2-379-2009, 2009.

Murtagh, D., Frisk, U., Merino, F., Ridal, M., Jonsson, A., Stegman, J., Witt, G., Eriksson, P., Jimenez, C., Megie, G., de la Noe, J., Ricaud, P., Baron, P., Pardo, J. R., Hauchcorne, A., Llewellyn, E. J., Degenstein, D. A., Gattinger, R. L., Lloyd, N. D., Evans, W. F. J., McDade, I. C., Haley, C. S., Sioris, C., von Savigny, C., Solheim, B. H., McConnell, J. C., Strong, K., Richardson, E. H., Leppelmeier, G. W., Kyrola, E., Auvinen, H., and Oikarinen, L.: An overview of the Odin atmospheric mission, Can. J. Phys., 80, 309–319, 2002.

Oltmans, S. H., Vömel, H., Hofmann, D., Rosenlof, K., and Kley, D.: The increase in stratospheric water vapor from balloonborne, frostpoint hygrometer measurements in Washington, D. C., and Boulder, Colorado, Geophys. Res. Lett., 27, 21, 3453–3456, doi:10.1029/2000GL012133, 2000.

Orsolini, Y. J., Urban, J., Murtagh, D. P., Lossow, S., and Limpasuvan, V.: Descent from the polar mesosphere and anomalously high stratopause observed in 8 years of water vapor and temperature satellite observations by the Odin Sub-Millimeter Radiometer, J. Geophys. Res., 115, D12305, doi:10.1029/2009JD013501, 2010.

Pitts, M. C., Thomason, L. W., Poole, L. R., and Winker, D. M.: Characterization of Polar Stratospheric Clouds with spaceborne

lidar: CALIPSO and the 2006 Antarctic season, Atmos. Chem. Phys., 7, 5207–5228, doi:10.5194/acp-7-5207-2007, 2007.

Pitts, M. C., Poole, L. R., and Thomason, L. W.: CALIPSO polar stratospheric cloud observations: second-generation detection algorithm and composition discrimination, Atmos. Chem. Phys., 9, 7577–7589, doi:10.5194/acp-9-7577-2009, 2009.

Pitts, M. C., Poole, L. R., Dörnbrack, A., and Thomason, L. W.: The 2009–2010 Arctic polar stratospheric cloud season: a CALIPSO perspective, Atmos. Chem. Phys., 11, 2161–2177, doi:10.5194/acp-11-2161-2011, 2011.

Randel, W. J., Wu, F., Oltmans, S. J., Rosenlof, K. and Nedoluha, G. E.: Interannual changes of stratospheric water vapor and correlations with tropical tropopause temperatures, J. Atmos. Sci., 61, 2133–2148, 2004.

Randel, W. J., Wu, F., Vömel, H., Nedoluha, G. E., and Forster, P.: Decreases in stratospheric water vapor after 2001: links to changes in the tropical tropopause and the Brewer–Dobson circulation, J. Geophys. Res., 111, D12312, doi:10.1029/2005JD006744, 2006.

Rex, M., Salawitch, R. J., Deckelmann, H., von der Gathen, P., Harris, N. P., Chipperfield, M. P., and Naujokat, B.: Arctic ozone loss and climate change, Geophys. Res. Lett., 31, L04116, doi:10.1029/2003GL018844, 2004.

Rex, M., Salawitch, R. J., Deckelmann, H., von der Gathen, P., Harris, N. P., Chipperfield, M. P., Naujokat, B., Reimer, E., Allaart, M., Andersen, S. B., Bevilacqua, R., Braathen, G. O., Claude, H., Davies, J., De Backer, H., Dier, H., Dorokhov, V., Fast, H., Gerding, M., Godin-Beekmann, S., Hoppel, K., Johnson, B., Kyrö, E., Litynska, Z., Moore, D., Nakane, H., Parrondo, M. C., Risley Jr., A. D., Skrivankova, P., Stubi, R., Viatte, P., Yushkov, V., and Zerefos, C.: Arctic winter 2005: implications for stratospheric ozone loss and climate change, Geophys. Res. Lett., 33, L23808, doi:10.1029/2006GL026731, 2006.

Rosenlof, K. H., Oltmans, S. J., Kley, D., Russell, J. M., Chiou, E. W., Chu, W. P., Johnson, D. G., Kelly, K. K., Michelsen, H. A., Nedoluha, G. E., Remsberg, E. E., Toon, G. C., and McCormick, M. P.: Stratospheric water vapor increases over the past half-century, Geophys. Res. Lett., 28, 1195–1198, doi:10.1029/2000GL012502, 2001.

Rozanov, A., Weigel, K., Bovensmann, H., Dhomse, S., Eichmann, K.-U., Kivi, R., Rozanov, V., Vömel, H., Weber, M., and Burrows, J. P.: Retrieval of water vapor vertical distributions in the upper troposphere and the lower stratosphere from SCIAMACHY limb measurements, Atmos. Meas. Tech., 4, 933–954, doi:10.5194/amt-4-933-2011, 2011.

Russell, J. M., Gordley, L. L., Park, J. H., Drayson, S. R., Tuck, A. F., Harries, J. E., Cicerone, R. J., Crutzen, P. J., and Frederick, J. E.: The halogen occultation experiment, J. Geophys. Res., 98, 10777–10797, 1993.

Santee, M. L., Read, W. G., Waters, J. W., Froidevaux, L., Manney, G. L., Flower, D. A., Jarnot, R. F., Harwood, R. S., and Peckham, G. E.: Interhemispheric differences in polar stratospheric HNO₃, H₂O, ClO, and O₃, Science, 267, 849–852, 1995.

Scherer, M., Vömel, H., Fueglistaler, S., Oltmans, S. J., and Staehelin, J.: Trends and variability of midlatitude stratospheric water vapour deduced from the re-evaluated Boulder balloon series and HALOE, Atmos. Chem. Phys., 8, 1391–1402, doi:10.5194/acp-8-1391-2008, 2008.

Shindell, D. T., Rind, D., and Lonergan, P.: Increased polar stratospheric ozone losses and delayed eventual recovery owing to increasing greenhouse-gas concentrations, Nature, 392, 589–592, 1998.

Sinnhuber, B.-M., Stiller, G., Ruhnke, R., von Clarmann, T., and Kellmann, S.: Arctic winter 2010/2011 at the brink of an ozone hole, Geophys. Res. Lett., 38, L24814, doi:10.1029/2011GL049784, 2011.

Solomon, S., Rosenlof, K. H., Portmann, R. W., Daniel, J. S., Davis, S. M., Sanford, T. J., and Plattner, G.-K.: Contributions of stratospheric water vapor to decadal changes in the rate of global warming, Science, 327, 1219–1223, doi:10.1126/science.1182488, 2010.

Sonkaew, T., von Savigny, C., Eichmann, K.-U., Weber, M., Rozanov, A., Bovensmann, H., Burrows, J. P., and Grooß, J.-U.: Chemical ozone losses in Arctic and Antarctic polar winter/spring season derived from SCIAMACHY limb measurements 2002–2009, Atmos. Chem. Phys., 13, 1809–1835, doi:10.5194/acp-13-1809-2013, 2013.

SPARC CCMVal: SPARC Report on the Evaluation of Chemistry-Climate Models, edited by: Eyring, V., Shepherd, T. G., and Waugh, D. W., SPARC Report No. 5, WCRP-132, WMO/TD-No. 1526, 2010.

Stiller, G. P., von Clarmann, T., Haenel, F., Funke, B., Glatthor, N., Grabowski, U., Kellmann, S., Kiefer, M., Linden, A., Lossow, S., and López-Puertas, M.: Observed temporal evolution of global mean age of stratospheric air for the 2002 to 2010 period, Atmos. Chem. Phys., 12, 3311–3331, doi:10.5194/acp-12-3311-2012, 2012.

Tabazadeh, A., Santee, M. L., Danilin, M. Y., Pumphrey, H. C., Newman, P. A., Hamill, P. J., and Mergenthaler, J. L.: Quantifying denitrification and its effect on ozone recovery, Science, 288, 1407–1411, 2000.

Urban, J.: Tropical ascent of lower stratospheric air analysed using measurements of the Odin Sub-Millimetre Radiometer, in: Proc. Reunion Island Int. Symp. Tropical Stratosphere Upper Troposphere, 5–9 November 2007, St. Gilles, Reunion Island, France, edited by: Bencherif, H., Universite de la Reunion, 2008.

Urban, J., Lautié, N., Le Flochmoën, E., Jiménez, C., Eriksson, P., De La Noë, J., Dupuy, E., Ekström, M., El Amraoui, L., Frisk, U., Murtagh, D., Olberg, M., and Ricaud, P.: Odin/SMR limb observations of stratospheric trace gases: level 2 processing of ClO, N₂O, HNO₃, and O₃, J. Geophys. Res., 110, D14307, doi:10.1029/2004JD005741, 2005a.

Urban, J., Lautié, N., Le Flochmoën, E., Jiménez, C., Eriksson, P., De La Noë, J., Dupuy, E., El Amraoui, L., Frisk, U., Jégou, F., Murtagh, D., Olberg, M., Ricaud, P., Camy-Peyret, C., Dufour, G., Payan, S., Huret, N., Pirre, M., Robinson, A. D., Harris, N. R. P., Bremer, H., Kleinböhl, A., Küllmann, K., Künzi, K., Kuttipurath, J., Ejiri, M. K., Nakajima, H., Sasano, Y., Sugita, T., Yokota, T., Piccolo, C., Raspollini, P., and Ridolfi, M.: Odin/SMR limb observations of stratospheric trace gases: validation of N₂O, J. Geophys. Res., 110, D09301, doi:10.1029/2004JD005394, 2005b.

Urban, J., Lautie, N., Murtagh, D., Eriksson, P., Kasai, Y., Lossow, S., Dupuy, E., de la Noe, J., Frisk, U., Olberg, M., Flochmoen, E. L., and Ricaud, P.: Global observations of middle atmospheric water vapour by the Odin satellite: an overview, Planet. Space Sci., 55, 1093–1102, 2007.

Urban, J., Murtagh, D. P., Stiller, G., and Walker, K. A.: Evolution and variability of water vapour in the tropical tropopause and lower stratosphere region derived from satellite measurements, in: Proceedings of the ESA Atmospheric Science Conference: Atmospheric Science and Applications, 18–22 June 2012, Brugge, Belgium, edited by: Ouwehand, L., ESA-SP-708, Eur. Space Agency Spec. Publ., ISBN/ISSN:978-92-9092-272-8, 2012.

Urban, J., Lossow, S., Stiller, G., and Read, W.: Another drop in water vapour, EOS, 95, 245–252, 2014.

Voigt, C., Schlager, H., Luo, B. P., Dörnbrack, A., Roiger, A., Stock, P., Curtius, J., Vössing, H., Borrmann, S., Davies, S., Konopka, P., Schiller, C., Shur, G., and Peter, T.: Nitric Acid Trihydrate (NAT) formation at low NAT supersaturation in Polar Stratospheric Clouds (PSCs), Atmos. Chem. Phys., 5, 1371-1380, doi:10.5194/acp-5-1371-2005, 2005.

von Clarmann, T., Höpfner, M., Kellmann, S., Linden, A., Chauhan, S., Funke, B., Grabowski, U., Glatthor, N., Kiefer, M., Schieferdecker, T., Stiller, G. P., and Versick, S.: Retrieval of temperature, H$_2$O, O$_3$, HNO$_3$, CH$_4$, N$_2$O, ClONO$_2$ and ClO from MIPAS reduced resolution nominal mode limb emission measurements, Atmos. Meas. Tech., 2, 159–175, doi:10.5194/amt-2-159-2009, 2009.

von Clarmann, T., Stiller, G., Grabowski, U., Eckert, E., and Orphal, J.: Technical Note: Trend estimation from irregularly sampled, correlated data, Atmos. Chem. Phys., 10, 6737–6747, doi:10.5194/acp-10-6737-2010, 2010.

von Hobe, M., Bekki, S., Borrmann, S., Cairo, F., D'Amato, F., Di Donfrancesco, G., Dörnbrack, A., Ebersoldt, A., Ebert, M., Emde, C., Engel, I., Ern, M., Frey, W., Genco, S., Griessbach, S., Grooß, J.-U., Gulde, T., Günther, G., Hösen, E., Hoffmann, L., Homonnai, V., Hoyle, C. R., Isaksen, I. S. A., Jackson, D. R., Jánosi, I. M., Jones, R. L., Kandler, K., Kalicinsky, C., Keil, A., Khaykin, S. M., Khosrawi, F., Kivi, R., Kuttippurath, J., Laube, J. C., Lefèvre, F., Lehmann, R., Ludmann, S., Luo, B. P., Marchand, M., Meyer, J., Mitev, V., Molleker, S., Müller, R., Oelhaf, H., Olschewski, F., Orsolini, Y., Peter, T., Pfeilsticker, K., Piesch, C., Pitts, M. C., Poole, L. R., Pope, F. D., Ravegnani, F., Rex, M., Riese, M., Röckmann, T., Rognerud, B., Roiger, A., Rolf, C., Santee, M. L., Scheibe, M., Schiller, C., Schlager, H., Siciliani de Cumis, M., Sitnikov, N., Søvde, O. A., Spang, R., Spelten, N., Stordal, F., Suminska-Ebersoldt, O., Ulanovski, A., Ungermann, J., Viciani, S., Volk, C. M., vom Scheidt, M., von der Gathen, P., Walker, K., Wegner, T., Weigel, R., Weinbruch, S., Wetzel, G., Wienhold, F. G., Wohltmann, I., Woiwode, W., Young, I. A. K., Yushkov, V., Zobrist, B., and Stroh, F.: Reconciliation of essential process parameters for an enhanced predictability of Arctic stratospheric ozone loss and its climate interactions (RECONCILE): activities and results, Atmos. Chem. Phys., 13, 9233–9268, doi:10.5194/acp-13-9233-2013, 2013.

Waters, J., Froidevaux, L., Harwood, R. S., Jarnot, R. F., Pickett, H. M., Read, W. G., Siegel, P. H., Cofield, R. E., Filipiak, M. J., Flower, D. A., Holden, J. R., Lau, G. K., Livesey, N. J., Manney, G. L., Pumphrey, H. C., Santee, M. L., Wu, D. L., Cuddy, D. T., Lay, R. R., Loo, M. S., Perun, V. S., Schwartz, M. J., Stek, P. C., Thurstans, R. P., Boyles, M. A., Chandra, K. M., Chavez, M. C., Chen, G. S., Chudasama, B. V., Dodge, R., Fuller, R. A., Girard, M. A., Jiang, J. H., Jiang, Y. B., Knosp, B. W., LaBelle, R. C., Lam, J. C., Lee, K. A., Miller, D., Oswald, J. E., Patel, N. C., Pukala, D. M., Quintero, O., Scaff, D. M., Van Snyder, W., Tope, M. C., Wagner, P. A., and Walch, M. J.: The Earth Observing System Microwave Limb Sounder (EOS MLS) on the Aura satellite, IEEE T. Geosci. Remote, 44, 1075–1092, 2006.

Weigel, K., Rozanov, A., Azam, F., Bramstedt, K., Damadeo, R., Eichmann, K.-U., Gebhardt, C., Hurst, D., Kraemer, M., Lossow, S., Read, W., Spelten, N., Stiller, G. P., Walker, K. A., Weber, M., Bovensmann, H., and Burrows, J. P.: UTLS water vapour from SCIAMACHY limb measurements V3.01 (2002–2012), Atmos. Meas. Tech. Discuss., 8, 7953–8021, doi:10.5194/amtd-8-7953-2015, 2015.

Winker, D. M., Hunt, W. H., and McGill, M.: Initial performance assessment of CALIOP, Geophys. Res. Lett., 34, L19803, doi:10.1029/2007GL030135, 2007.